Inorg. Chem. **2006**, *45*, 2795–2811

Spectroscopic Properties and Electronic Structure of Five- and Six-Coordinate Iron(II) Porphyrin NO Complexes: Effect of the Axial N-Donor Ligand

V. K. K. Praneeth, Christian Näther, Gerhard Peters, and Nicolai Lehnert*

Institut für Anorganische Chemie, Christian-Albrechts-Universität Kiel, Olshausenstrasse 40, D-24098 Kiel, Germany

Received May 30, 2005

In this paper, the differences in the spectroscopic properties and electronic structures of five- and six-coordinate iron(II) porphyrin NO complexes are explored using [Fe(TPP)(NO)] (**1**; TPP = tetraphenylporphyrin) and [Fe(TPP)(MI)(NO)] (**2**; MI = 1-methylimidazole) type systems. Binding of N-donor ligands in axial position trans to NO to five-coordinate complexes of type **1** is investigated using UV–vis absorption and ^{1}H NMR spectroscopies. This way, the corresponding binding constants K_{eq} are determined and the ^{1}H NMR spectra of **1** and **2** are assigned for the first time. In addition, ^{1}H NMR allows for the determination of the degree of denitrosylation in solutions of **1** with excess base. The influence of the axial ligand on the properties of the coordinated NO is then investigated. Vibrational spectra (IR and Raman) of **1** and **2** are presented and assigned using isotope substitution and normal-coordinate analysis. Obtained force constants are 12.53 (N–O) and 2.98 mdyn/Å (Fe–NO) for **1** compared to 11.55 (N–O) and 2.55 mdyn/Å (Fe–NO) for **2**. Together with the NMR results, this provides experimental evidence that binding of the trans ligand weakens the Fe–NO bond. The principal bonding schemes of **1** and **2** are very similar. In both cases, the Fe–N–O subunit is strongly bent. Donation from the singly occupied π^* orbital of NO into d_{z^2} of iron(II) leads to the formation of an Fe–NO σ bond. In addition, a medium-strong π back-bond is present in these complexes. The most important difference in the electronic structures of **1** and **2** occurs for the Fe–NO σ bond, which is distinctively stronger for **1** in agreement with the experimental force constants. The increased σ donation from NO in **1** also leads to a significant transfer of spin density from NO to iron, as has been shown by magnetic circular dichroism (MCD) spectroscopy in a preceding Communication (Praneeth, V. K. K.; Neese, F.; Lehnert, N. *Inorg. Chem.* **2005**, *44*, 2570–2572). This is confirmed by the ^{1}H NMR results presented here. Hence, further experimental and computational evidence is provided that complex **1** has noticeable $Fe^{I}NO^{+}$ character relative to **2**, which is an $Fe^{II}NO$(radical) complex. Finally, using MCD theory and quantum chemical calculations, the absorption and MCD **C**-term spectra of **1** and **2** are assigned for the first time.

Introduction

Iron porphyrin NO complexes play a key role in the mechanisms of many metalloproteins.[1] These include nitrite and nitric oxide reductases (NIRs and NORs, denitrification),[2] NO receptors in neural signaling,[3] NO carriers in bloodsucking insects (nitrophorins),[4] nitric oxide synthase,[5] and guanylate cyclase.[6] Among the different hemes investigated, the NO adducts of hemoglobin and myoglobin are probably some

* To whom correspondence should be addressed. E-mail: nlehnert@ac.uni-kiel.de.

(1) McCleverty, J. A. *Chem. Rev.* **2004**, *104*, 403−418.

(2) (a) Ferguson, S. J. *Curr. Opin. Chem. Biol.* **1998**, *2*, 182−193. (b) Richardson, D. J.; Watmough, N. J. *Curr. Opin. Chem. Biol.* **1999**, *3*, 207−219. (c) Moura, I.; Moura, J. J. G. *Curr. Opin. Chem. Biol.* **2001**, *5*, 168−175.

(3) (a) Moncada, S.; Palmer, R. M. J.; Higgs, E. A. *Pharmacol. Rev.* **1991**, *43*, 109−142. (b) Bredt, D. S.; Snyder, S. H. *Annu. Rev. Biochem.* **1994**, *63*, 175−195.

(4) (a) Ribeiro, J. M. C.; Hazzard, J. M. H.; Nussenzveig, R. H.; Champagne, D. E.; Walker, F. A. *Science* **1993**, *260*, 539−541. (b) Ding, X. D.; Weichsel, A.; Andersen, J. F.; Shokhireva, T. K.; Balfour, C.; Pierik, A. J.; Averill, B. A.; Montfort, W. R.; Walker, F. A. *J. Am. Chem. Soc.* **1999**, *121*, 128−138. (c) Walker, F. A. *J. Inorg. Biochem.* **2005**, *99*, 216−236.

(5) (a) Stuehr, D. J. *Annu. Rev. Pharmacol. Toxicol.* **1997**, *37*, 339−359. (b) Poulos, T. L.; Li, H.; Raman, C. S. *Curr. Opin. Chem. Biol.* **1999**, *3*, 131−137. (c) Li, H.; Poulos, T. L. *J. Inorg. Biochem.* **2005**, *99*, 293−305.

10.1021/ic050865j CCC: $33.50
Published on Web 02/28/2006

Scheme 1

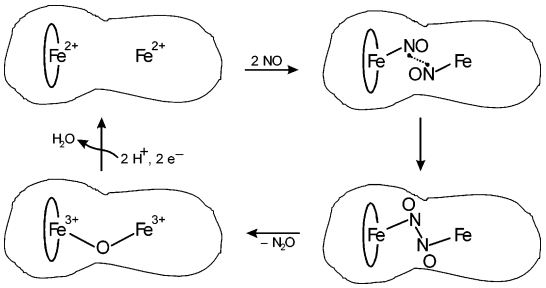

of the most-studied systems in biology.[7] Many of these proteins that have been studied contain iron porphyrin centers with axial histidine ligation. Corresponding iron(II) porphyrin NO complexes occur as intermediates in bacterial NOR.[8] This enzyme reduces nitric oxide to nitrous oxide at an active site that contains both an iron porphyrin and a nonheme iron center in close proximity. The proposed mechanism includes binding of two molecules of NO (one at each of the two metal centers) followed by N−N coupling of the two NO units as the central step of catalysis (cf. Scheme 1).[9] However, evidence to prove this mechanism is still lacking and, in addition, other investigations have led to different mechanistic possibilities as well.[10] It is, therefore, of central importance to define the electronic structure of the iron(II) porphyrin NO adducts in detail to obtain further insight into the catalytic mechanism of this enzyme. In the case of soluble guanylate cyclase, a five-coordinate (5C) ferrous heme with axial histidine is present in the active site, which, upon coordination of NO, forms a 5C NO adduct where histidine is no longer bound to the iron(II) center. This triggers a conformational change that activates the enzyme. Because of this general importance of iron porphyrin NO adducts, a large amount of research has been conducted toward the synthesis of corresponding model complexes. These investigations use synthetic porphyrin ligands such as tetraphenylporphyrin (TPP) or octaethylporphyrin (OEP). Most of the research is focused on either 5C species [Fe(porphyrin)(NO)]$^{n+}$ ($n = 0$ and 1) or corresponding six-coordinate (6C) complexes with N-donor ligands such as imidazole, pyridine (Py), piperidine, etc., in the position trans to NO.[11] Corresponding iron(II) model complexes are still the focus of many ongoing studies because of their interesting spectroscopic and photochemical properties[12] and their mechanistic significance.[10c,11a,13] From crystallography, these systems are characterized by short Fe−N(O) distances of about 1.75 Å and bent Fe−NO units with an Fe−N−O angle of about 140°.[14,15] Importantly, electron paramagnetic resonance (EPR) spectroscopic studies revealed interesting differences between the 5C and 6C iron(II) porphyrin NO adducts:[16] 5C complexes show a characteristic spectrum with hyperfine lines from the nitrogen of NO on the smallest *g* value, *g*(min), whereas corresponding 6C complexes show a broader spectrum, where hyperfine lines are now observed for the nitrogens of NO and of the *trans*-N donor on *g*(mid). These differences in the EPR spectra are due to different orientations of the *g* tensor in these complexes.[14,17] From vibrational spectroscopy, the 5C iron(II) porphyrin NO adduct [Fe(TPP)(NO)] (**1**) has an N−O stretching frequency of about 1700 cm^{-1}, whereas the corresponding 6C complex [Fe(TPP)(MI)(NO)] (**2**) with 1-methylimidazole (MI) as the axial ligand shows ν(NO) at about 1630 cm^{-1}.[11b,16a,18] Despite the large amount of experimental data available for these systems, their exact electronic structures are still not clearly defined. This is due to the fact that NO is a redox-active ligand, which complicates the exact determination of the electronic structure and the assignment of (formal) oxidation states.[19] A number of density functional theory (DFT) studies have focused on these complexes, and different electronic structures have been obtained from these calculations.[17,20] In a recent paper, we have used magnetic circular dichroism (MCD) spectroscopy[21] coupled with DFT calculations to elucidate the differences in the electronic structures of 5C and 6C iron(II) porphyrin

(6) (a) Garbers, D. L.; Lowe, D. G. *J. Biol. Chem.* **1994**, *269*, 30741−30744. (b) Zhao, Y.; Hoganson, C.; Babcock, G. T.; Marletta, M. A. *Biochemistry* **1998**, *37*, 12458−12464.
(7) Møller, J. K. S.; Skibsted, L. H. *Chem. Rev.* **2002**, *102*, 1167−1178.
(8) Wasser, I. M.; de Vries, S.; Moënne-Loccoz, P.; Schröder, I.; Karlin, K. D. *Chem. Rev.* **2002**, *102*, 1201−1234.
(9) Girsch, P.; de Vries, S. *Biochim. Biophys. Acta* **1997**, *1318*, 202−216.
(10) (a) Butler, C. S.; Seward, H. E.; Greenwood, C.; Thomson, A. J. *Biochemistry* **1997**, *36*, 16259−16266. (b) Watmough, N. J.; Cheesman, M. R.; Butler, C. S.; Little, R. H.; Greenwood, C.; Thomson, A. J. *J. Bioenerg. Biomembr.* **1998**, *30*, 55−62. (c) Lin, R.; Farmer, P. J. *J. Am. Chem. Soc.* **2001**, *123*, 1143−1150.
(11) (a) Ford, P. C.; Lorkovic, I. M. *Chem. Rev.* **2002**, *102*, 993−1017. (b) Wyllie, G. R. A.; Scheidt, R. *Chem. Rev.* **2002**, *102*, 1067−1089. (c) Walker, F. A.; Simonis, U. Iron Porphyrin Chemistry. In *Encyclopedia of Inorganic Chemistry*; Bruce, R. B., Ed.; Wiley: New York, 2005.
(12) (a) Zavarine, I. S.; Kini, A. D.; Morimoto, B. H.; Kubiak, C. P. *J. Phys. Chem. B* **1998**, *102*, 7287−7292. (b) Cheng, L.; Novozhilova, I.; Kim, C.; Kovalevsky, A.; Bagley, K. A.; Coppens, P.; Richter-Addo, G. B. *J. Am. Chem. Soc.* **2000**, *122*, 7142−7143. (c) Lee, J.; Kovalevsky, A. Y.; Novozhilova, I. V.; Bagley, K. A.; Coppens, P.; Richter-Addo, G. B. *J. Am. Chem. Soc.* **2004**, *126*, 7180−7181.
(13) (a) Lorković, I. M.; Ford, P. C. *Inorg. Chem.* **1999**, *38*, 1467−1473. (b) Kurtikyan, T. S.; Martirosyan, G. G.; Lorković, I. M.; Ford, P. C. *J. Am. Chem. Soc.* **2002**, *124*, 7180−7181. (c) Lim, M. D.; Lorković, I. M.; Wedeking, K.; Zanella, A. W.; Works, C. F.; Massick, S. M.; Ford, P. C. *J. Am. Chem. Soc.* **2002**, *124*, 9737−9743. (d) Patterson, J. C.; Lorković, I. M.; Ford, P. C. *Inorg. Chem.* **2003**, *42*, 4902−4908. (e) Lim, M. D.; Lorković, I. M.; Ford, P. C. *J. Inorg. Biochem.* **2005**, *99*, 151−165.
(14) Wyllie, G. R. A.; Schulz, C. E.; Scheidt, W. R. *Inorg. Chem.* **2003**, *42*, 5722−5734.
(15) Scheidt, W. R.; Ellison, M. K. *Acc. Chem. Res.* **1999**, *32*, 350−359.
(16) (a) Wayland, B. B.; Olson, L. W. *J. Am. Chem. Soc.* **1974**, *96*, 6037−6041. (b) Morse, R. H.; Chan, S. I. *J. Biol. Chem.* **1980**, *255*, 7876−7882. (c) Hüttermann, J.; Burgard, C.; Kappl, R. *J. Chem. Soc., Faraday Trans.* **1994**, *90*, 3077. (d) Hayes, R. G.; Ellison, M. K.; Scheidt, W. R. *Inorg. Chem.* **2000**, *39*, 3665−3668
(17) Patchkovskii, S.; Ziegler, T. *Inorg. Chem.* **2000**, *39*, 5354−5364.
(18) Praneeth, V. K. K.; Neese, F.; Lehnert, N. *Inorg. Chem.* **2005**, *44*, 2570−2572.
(19) Westcott, B. L.; Enemark, J. H. *Transition Metal Nitrosyls*; Solomon, E. I., Lever, A. B. P., Eds.; Wiley: New York, 1999; Vol. 2, pp 403−450.
(20) (a) Rovira, C.; Kunc, K.; Hutter, J.; Ballone, P.; Parrinello, M. *J. Phys. Chem. A* **1997**, *101*, 8914−8925. (b) Ghosh, A.; Wondimagegn, T. *J. Am. Chem. Soc.* **2000**, *122*, 8101−8102. (c) Zhang, Y.; Mao, J.; Godbout, N.; Oldfield, E. *J. Am. Chem. Soc.* **2002**, *124*, 13921−13930. (d) Zhang, Y.; Gossman, W.; Oldfield, E. *J. Am. Chem. Soc.* **2003**, *125*, 16387−16396.
(21) (a) Cheesman, M. R.; Greenwood, C.; Thomson, A. J. *Adv. Inorg. Chem.* **1991**, *36*, 201−255. (b) Solomon, E. I.; Pavel, E. G.; Loeb, K. E.; Campochiaro, C. *Coord. Chem. Rev.* **1995**, *144*, 369−460. (c) Neese, F.; Solomon, E. I. *Inorg. Chem.* **1999**, *38*, 1847−1865. (d) Oganesyan, V. S.; George, S. J.; Cheesman, M. R.; Thomson, A. J. *J. Chem. Phys.* **1999**, *110*, 762−777. (e) Lehnert, N.; DeBeer George, S.; Solomon, E. I. *Curr. Opin. Chem. Biol.* **2001**, *5*, 176−187.

NO adducts.[18] It was shown that, in the 5C complex **1**, a strong Fe−NO σ bond is present that leads to a large transfer of spin density from the NO ligand to Fe^{II} corresponding to an electronic structure with considerable $Fe^{I}NO^{+}$ character. In the 6C complex **2**, on the other hand, the spin density is pushed back from the iron toward the NO ligand, resulting in an Fe^{II}NO(radical)-type electronic structure. Calculated *g* tensors are in agreement with this description.[18] In recent studies, calculated *g* values and ^{14}N and ^{57}Fe hyperfine tensors (the latter are available from Mössbauer experiments[14]) have also been used to explore the structural flexibility of the NO ligand coordinated to ferrous heme.[17,20d] These results reveal another important property of iron(II) porphyrin NO adducts, i.e., that the orientation of the NO ligand is undefined at higher temperatures in these complexes because of low barriers for a rotation of NO around the Fe−N(O) bond.[22]

In this study, the spectroscopic properties and the electronic structures of 5C and 6C iron(II) porphyrin NO adducts are further elaborated in detail. Binding studies of N-donor ligands (L) to 5C complexes [Fe(TPP*)(NO)] (TPP* = tetraphenylporphyrin-type ligand) in solution as a function of the phenyl ring substitution in TPP and the employed nitrogen base are presented using UV−vis absorption and ^{1}H NMR spectroscopy. This way, binding constants K_{eq} are determined and the ^{1}H NMR spectra of these complexes are assigned for the first time. A crystal structure of the complex [Fe^{II}(T*o*-F_2PP)(MI)(NO)] (**2-F**; T*o*-F_2PP = tetrakis(*o*-difluorophenyl)porphyrin) is presented. The differences in the electronic structures of 5C and 6C iron(II) porphyrin NO complexes are then investigated by vibrational spectroscopy on [Fe(TPP)(NO)] (**1**) and [Fe(TPP)(MI)(NO)] (**2**) as examples. The vibrations of the Fe^{II}−N−O subunits in **1** and **2** are completely assigned for the first time using isotope substitution. Force constants are determined using quantum-chemistry-centered normal-coordinate analysis (QCC-NCA). The obtained force constants together with the ^{1}H NMR results provide direct experimental evidence for a weakening of the Fe−NO bond in 6C compared to 5C Fe^{II}NO complexes. In addition, the MCD spectra of **1** and **2**, which have been reported in a preceding Communication,[18] are assigned using MCD theory and quantum-chemical calculations. On the basis of all these spectroscopic results, which are correlated to the DFT calculations, the electronic structural differences between 5C and 6C iron(II) porphyrin NO adducts are now defined in detail.

Experimental and Computational Procedures

Syntheses. Reactions were performed by applying Schlenk techniques using carefully purified solvents. NO gas was passed through a potassium hydroxide column and then through a cold trap at −80 °C prior to usage to remove higher nitrogen oxide impurities.

Syntheses of Ligands. Tetraphenylporphyrin (H_2TPP),[23] tetramesitylporphyrin (H_2TMP),[24] and tetrakis(*o*-difluorophenyl)-porphyrin (H_2T*o*-F_2PP)[25] were synthesized and purified as previously reported.

Syntheses of Precursors. [Fe(TPP)Cl] and [Fe(TMP)Cl] were prepared according to the method of Adler et al.[26] [Fe(T*o*-F_2PP)Cl] was prepared by literature methods.[25]

Syntheses of Ferrous NO Adducts. The complexes [Fe(TPP*)(NO)] and [Fe(TPP*)(MI)(NO)] (TPP* = TPP, TMP, T*o*-F_2PP; MI = 1-methylimidazole) were synthesized using published procedures[14,27] and isolated as microcrystalline solids.[28] The identities of the compounds were established using elemental analysis, vibrational spectroscopy, and EPR.

Crystals of [Fe(T*o*-F_2PP)(MI)(NO)] suitable for X-ray analysis were prepared as follows. A sample of [Fe(T*o*-F_2PP)Cl] (20 mg) in a glass tube was placed inside a 150-mL Schlenk tube (equipped with a rubber septum) under an argon atmosphere. A total of 5 mL of $CHCl_3$ and 1 mL of MI were added to [Fe(T*o*-F_2PP)Cl], and the resulting solution was stirred for a few minutes. NO gas was passed through the Schlenk tube for 10 min, and the reaction mixture was further stirred for 30 min. *n*-Hexane (20 mL) was then introduced into the Schlenk tube outside of the glass tube for vapor diffusion. The Schlenk tube was sealed, and crystals of [Fe(T*o*-F_2PP)(MI)(NO)] were formed after 10 days.

Crystal Structure Determination. Intensity data were collected using a STOE Image Plate Diffraction System with Mo Kα radiation. The structure was solved with direct methods using *SHELXS-97*,[29] and refinement was done against F^2 using *SHELXS-97*.[29] All non-hydrogen atoms except O1A were refined with anisotropic displacement parameters. The hydrogen atoms were placed in ideal positions and were refined isotropically using the riding model. The oxygen atom is disordered in two positions and, therefore, refinement was performed using a split model. The lower occupied oxygen position (sof O1A = 0.1) was refined only isotropically (see the Supporting Information). Selected crystallographic data are presented in Table 1.

UV−Vis Spectroscopy. Absorption spectra were recorded in CH_2Cl_2 or toluene solutions as indicated at room temperature using a Varian Cary 5 UV−vis−near-infrared (NIR) spectrometer.

Vibrational Spectroscopy. Resonance Raman spectra were measured on a Dilor XY Raman spectrograph with a triple monochromator and a CCD detector. An Ar/Kr mixed-gas laser with a maximum power of 5 W was used for excitation. Spectra were recorded at excitation wavelengths of 454.5, 488.0, 514.5, 568.2, and 647.1 nm. The spectra were measured on KBr disks cooled to 10 K with a helium cryostat. The spectral band-pass was set to 2 cm^{-1}. Middle- and far-infrared spectra (MIR and FIR) were recorded on a Bruker IFS 66v vacuum instrument at room temperature. For the MIR region, KBr disks were used and the spectra were recorded at a resolution of 1 cm^{-1}. In the FIR region, CsI disks were applied and the resolution was set to 2 cm^{-1}. Low-

(22) Zemojtel, T.; Rini, M.; Heyne, K.; Dandekar, T.; Nibbering, E. T. J.; Kozlowski, P. M. *J. Am. Chem. Soc.* **2004**, *126*, 1930−1931.
(23) Adler, A. D.; Longo, F. R.; Finarrelli, J. F.; Goldmacher, J.; Assour, J.; Korsakoff, L. *J. Org. Chem.* **1967**, *32*, 476.
(24) Safo, M. K.; Gupta, G. P.; Walker, F. A.; Scheidt, W. R. *J. Am. Chem. Soc.* **1991**, *113*, 5497−5510.
(25) Ghiladi, R. A.; Kretzer, R. M.; Guzei, I.; Rheingold, A. L.; Neuhold, Y. M.; Hatwell, K. R.; Zuberbühler, A. D.; Karlin, K. D. *Inorg. Chem.* **2001**, *40*, 5754−5767.
(26) Adler, A. D.; Longo, F. R.; Kampas, F.; Kim, J. *J. Inorg. Nucl. Chem.* **1970**, *32*, 2443−2445.
(27) Scheidt, W. R.; Frisse, M. E. *J. Am. Chem. Soc.* **1975**, *97*, 17−21.
(28) Under the identical reaction conditions employed for the syntheses of 6C Fe^{II}NO complexes in this study, complexes **2** and **2-F** were prepared by very slow crystallization and obtained as pure materials. However, the isolation of the pure 6C complex using TMP as the ligand was unsuccessful and always yielded mixtures of **1-Me** and [Fe(TMP)(MI)(NO)] as evidenced by IR spectroscopy.
(29) Sheldrick, W. S. *SHELXS-97 and SHELXL-97: programs for the solution and refinement of crystal structures*; University of Göttingen: Göttingen, Germany, 1997.

Table 1. Crystallographic Data for Compound **2-F**[a]

chemical formula	$C_{51}H_{33}F_8N_7OFe$
fw	967.69
space group	$P2_1/c$
a, Å	13.126(1)
b, Å	12.885(1)
c, Å	25.803(2)
β, deg	96.07(1)
V, Å^3	4339.6(5)
T, K	293
Z	4
D_{calcd}	1.481
μ, mm^{-1}	0.431
λ, Å	0.71073
measured reflns	33628
independent reflns	8143
R_{int}	0.031
observed reflns	6593
R1 [$I > 2\sigma(I)$]	0.0370
wR2 (all data)	0.1009

[a] $R1 = \sum||F_o| - |F_c||/\sum|F_o|$; $wR2 = [\sum[w(F_o^2 - F_c^2)^2]/\sum[w(F_o^2)^2]]^{1/2}$.

temperature MIR spectra were obtained on a Mattson Genesis type I spectrometer equipped with a cryogenic CTI cryostat. Spectra were recorded at 20 K at a resolution of 1 cm^{-1}.

NMR Spectroscopy. ^{1}H NMR spectra of the iron(II) porphyrin NO complexes were recorded in CD_2Cl_2 on a Bruker Avance 400 pulse Fourier transform spectrometer operating at a ^{1}H NMR frequency of 400.13 MHz. The spectrum of [Fe(TPP)(Pip)$_2$] (where Pip is piperidine-d_{11}) was recorded by dissolution of [Fe(TPP)] in benzene-d_6 and addition of Pip. For the titration experiments, commercially available Pip was used because in this case the ~2% undeuterated solvent present does not show signals in the aromatic region.

MCD Spectroscopy. MCD spectra have been obtained on frozen glasses of butyronitrile/propionitrile (1:1 ratio) solutions in the 1.8−25 K temperature range. A CD spectropolarimeter (Jasco 810) with S1 and S20 photomultiplier tubes as detectors has been used in which the sample compartment was modified to accommodate an Oxford instruments SM4-10T magnetocryostat. The samples were frozen in metallic sample compartments between two Infrasil quartz disks separated by 3 mm neoprene spacers.

Normal-Coordinate Analysis (NCA). NCA calculations were performed using the QCPE computer program 576 by M. R. Peterson and D. F. McIntosh. The calculations are based on a general valence force field; force constants are refined with a nonlinear simplex algorithm. The simplex optimization was used to refine only *selected* force constants according to the quantum-chemical-assisted NCA (QCA-NCA) scheme.[30] Here, a force field from DFT calculations is used as a starting point to generate initial force constants, and a subset of these is fit to reproduce the known experimental frequencies. We have now fully interfaced the Gaussian output with the NCA software using a modified version of the program Redong[31] (QCPE 628). This new version produces input files that can directly be processed by the NCA programs. Compared to the QCA-NCA procedure,[30a] this allows for the routine treatment of very large systems because no simplifications have to be applied to the molecule or the force field. On the other hand, compared to the QCB-NCA version,[30b] the tedious editing of the input files is no longer necessary. This new version is called quantum-chemistry-centered normal-coordinate analysis (QCC-NCA) because it is designed for the treatment of large molecules where >99% of the force constants are purely computational.

DFT Calculations. The structures of the models [Fe(P)(NO)] ($\tilde{\mathbf{1}}$; $S = {}^1/_2$) and [Fe(P)(MI)(NO)] ($\tilde{\mathbf{2}}$; $S = {}^1/_2$) (where P is porphine) have been fully optimized using BP86/TZVP. For all of these calculations, a simplified TPP ligand has been used in which the four phenyl groups in the meso position of the porphyrin ring have been replaced by hydrogen. The resulting porphyrin model ligand P (P = porphine^{2-}) is shown in Figure 4 along with the coordinate system used. Vibrational frequencies have been calculated for all structures showing no imaginary frequencies. In addition, B3LYP/LanL2DZ* calculations have been performed on these systems to obtain accurate total energies and spin densities. The LanL2DZ* basis set consists of LanL2DZ plus polarization functions (from TZVP) on all heavy atoms. These methods were used as implemented in *Gaussian 98* (G98).[32] Absorption spectra of $\tilde{\mathbf{1}}$ and $\tilde{\mathbf{2}}$ were calculated using either time-dependent (TD-) DFT (G98) or the semiempirical INDO/S-CI method (active space: 160 orbitals) as implemented in *ORCA*.[33] EPR and Mössbauer parameters have also been calculated using *ORCA* and applying the B3LYP functional together with the following basis sets: Fe, CP(PPP); N, EPR-II; C and O, TZVP; H, TZV. Calculated Mössbauer isomer shifts (cf. Table S3 in the Supporting Information) were obtained after scaling the Fermi contact contribution to the ^{57}Fe hyperfine tensor with a factor of 1.81 as determined empirically.[34]

Results and Analysis

A. Binding of Axial N-Donor Ligands to Five-Coordinate Iron(II) Porphyrin NO Adducts. The binding of N-donor ligands to [Fe(TPP*)(NO)] in axial position trans to NO is studied in solution using UV−vis absorption and ^{1}H NMR spectroscopy. Importantly, the adduct of [Fe(T*o*-F$_2$PP)(NO)] (**1-F**) with MI has by far the largest binding constant K_{eq} of all systems investigated. To examine whether the increased K_{eq} structurally influences the Fe−NO bond, the crystal structure of the product **2-F** has been determined. Vibrational spectra of [Fe(TPP)(NO)] (**1**) and [Fe(TPP)(MI)(NO)] (**2**) are then presented and analyzed using isotope substitution and NCA.

A.1. Ligand Binding to [Fe(TPP*)(NO)] Complexes in Solution Monitored by UV−Vis Absorption Spectroscopy. The coordination of the N-donor ligands 1-methylimidazole (MI) and pyridine (Py) to the five-coordinate (5C) complexes **1**, [Fe(TMP)(NO)] (**1-Me**), and **1-F** is studied in solution using UV−vis absorption spectroscopy in order to determine the equilibrium constants K_{eq} of the reaction

$$[Fe(TPP^*)(NO)] + L \leftrightarrow [Fe(TPP^*)(L)(NO)] \qquad (1)$$

(30) (a) Lehnert, N.; Tuczek, F. *Inorg. Chem.* **1999**, *38*, 1659−1670. (b) Studt, F.; MacKay, B. A.; Fryzuk, M. D.; Tuczek, F. *J. Am. Chem. Soc.* **2004**, *126*, 280−290.
(31) Allouche, A.; Pourcin, J. *Spectrochim. Acta A* **1993**, *49*, 571.
(32) Frisch, M. J.; Trucks, G. W.; Schlegel, H. B.; Scuseria, G. E.; Robb, M. A.; Cheeseman, J. R.; Zakrzewski, V. G.; Montgomery, J. A., Jr.; Stratmann, R. E.; Burant, J. C.; Dapprich, S.; Millam, J. M.; Daniels, A. D.; Kudin, K. N.; Strain, M. C.; Farkas, O.; Tomasi, J.; Barone, V.; Cossi, M.; Cammi, R.; Mennucci, B.; Pomelli, C.; Adamo, C.; Clifford, S.; Ochterski, J.; Petersson, G. A.; Ayala, P. Y.; Cui, Q.; Morokuma, K.; Salvador, P.; Dannenberg, J. J.; Malick, D. K.; Rabuck, A. D.; Raghavachari, K.; Foresman, J. B.; Cioslowski, J.; Ortiz, J. V.; Baboul, A. G.; Stefanov, B. B.; Liu, G.; Liashenko, A.; Piskorz, P.; Komaromi, I.; Gomperts, R.; Martin, R. L.; Fox, D. J.; Keith, T.; Al-Laham, M. A.; Peng, C. Y.; Nanayakkara, A.; Challacombe, M.; Gill, P. M. W.; Johnson, B.; Chen, W.; Wong, M. W.; Andres, J. L.; Gonzalez, C.; Head-Gordon, M.; Replogle, E. S.; Pople, J. A. *Gaussian 98*, revision A.11; Gaussian, Inc.: Pittsburgh, PA, 2001.
(33) Neese, F. *ORCA*, version 2.2; Max-Planck Institut für Bioanorganische Chemie: Mülheim/Ruhr, Germany, 2004.

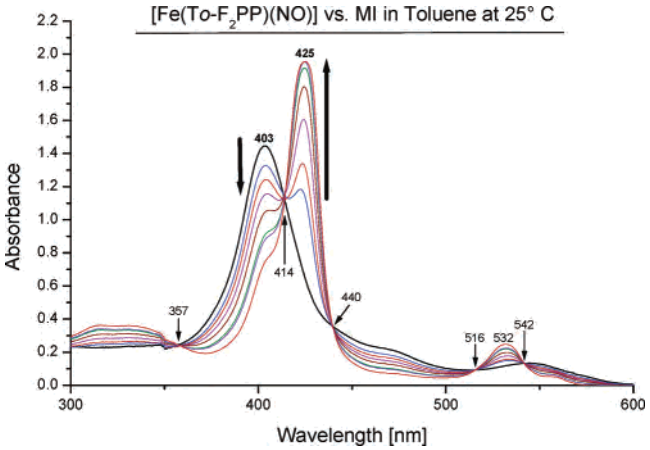

Figure 1. Titration of [Fe(To-F_2PP)(NO)] (**1-F**) with 1-methylimidazole (MI) in a toluene solution at room temperature monitored by UV−vis absorption spectroscopy. The Soret band of **1-F** at 403 nm disappears, while the Soret band of the product **2-F** appears at 425 nm.

Figure 1 shows a typical plot of the titration of a 5C iron(II) porphyrin NO adduct with an N-donor ligand. In this case, **1-F** was used and reacted with MI. The initial spectrum of the 5C species shows a broad peak in the Soret region centered at 403 nm. Upon the addition of the ligand, this peak decreases in intensity, whereas a band at 425 nm appears, which corresponds to the Soret band of the obtained six-coordinate (6C) complex **2-F**. Isosbestic points (cf. Figure 1) indicate that this reaction corresponds to a clean transformation of **1-F** to **2-F** without further intermediates. In the case of simple ligand binding reactions such as eq 1, the equilibrium constant K_{eq} can be determined from the equation

$$c(\mathrm{B})^0 = c_T \Delta\epsilon \frac{c(\mathrm{B})^0}{\Delta E} - K_{eq}^{-1} \qquad (2)$$

which is based on a general expression that was first derived by Drago and co-workers.[35,36] UV−vis absorption measurements are performed at different concentrations $c(\mathrm{B})^0$ of base, and the change in absorbance ΔE is measured. A plot of $c(\mathrm{B})^0$ vs $c(\mathrm{B})^0/\Delta E$ then gives K_{eq}^{-1}. The advantage of this method is that the absolute concentrations of the 5C and 6C complexes do not need to be determined. Several important trends can be derived from the resulting K_{eq} values listed in Table 2. For ligand TPP (complex **1**), equilibrium constants of 26 M^{-1} for MI and 3 M^{-1} for Py have been determined, which correspond to a weak interaction. Correspondingly, the free binding energies $\Delta G°$ range in the region of only −1 to −5 kcal/mol. This is in agreement with the experimental finding that the isolation of 6C complexes [Fe(TPP*)(L)(NO)] is difficult.[14] The obtained K_{eq} for Py is in good agreement with the literature value of 0.7 M^{-1} obtained in an ethylene chloride solution.[37] The lower binding constant of Py compared to MI can be rationalized with Py being a weaker base ($pK_B = 8.75$) than MI ($pK_B = 6.67$). From Table 2, K_{eq} increases in the order **1** < **1-Me** < **1-F**. Hence, ortho substitution of the phenyl rings of TPP leads to an increase in the binding constant. This is also observed for the coordination of N-donor ligands to [Fe(TPP*)]-type complexes[11c] and can be attributed to steric shielding of the binding site.[38] In addition, the electron-withdrawing fluoro substituents in To-F_2PP lead to a further stabilization of the adducts compared to methyl groups in TMP. However, the fluoro substitution of TPP has a distinctively different effect on K_{eq} for MI and Py: compared to TPP, *usage of To-F_2PP leads to an increase in the binding constant for MI by a factor of 80*, whereas for Py, the increase is only by a factor of 2.3. This is attributed to the fact that MI has π-donor properties, whereas Py is a π acceptor. Hence, the withdrawal of electron density from the porphyrin leads to an increase in binding for MI because of electronic effects, whereas the Py adduct only experiences a small stabilization because of steric and/or electrostatic effects. To further evaluate this result, we isolated complex [Fe(To-F_2PP)(MI)(NO)] (**2-F**) as a solid. Importantly, a solution of solid **2-F** in toluene or benzene leads to the UV−vis absorption spectrum shown in Figure S5 in the Supporting Information, which resembles the spectrum of the corresponding 6C complex obtained from solutions of **1-F** with excess MI. In contrast, the solution spectra of solid **2** and **2-Me** resemble the data of the corresponding 5C complexes indicative of the much smaller binding constants in these cases. Hence, the combination of To-F_2PP and MI seems to be ideal for the preparation of 6C $Fe^{II}NO$ complexes in solution.

Table 2. Calculated Equilibrium Constants K_{eq} [M^{-1}] and Free Reaction Energies $\Delta G°$ [kcal/mol] for the Reaction of [Fe(TPP*)(NO)] with N-Donor Ligands Following Equation 1

	equilib constant K_{eq}		$\Delta G° = -RT \ln(K_{eq})$	
complex	MI	Py	MI	Py
[Fe(TPP)(NO)] (**1**)	26	3	−1.9	−0.7
[Fe(TMP)(NO)] (**1-Me**)	36		−2.1	
[Fe(To-F_2PP)(NO)] (**1-F**)	2055	7	−4.5	−1.2

A.2. Ligand Binding to [Fe(TPP*)(NO)] Complexes in Solution Monitored by NMR Spectroscopy. As shown in section A.1, UV−vis spectroscopy is a useful tool to monitor the binding of axial N-donor ligands to 5C complexes [Fe(TPP*)(NO)]. However, there is a potential problem: because of the large concentrations of base often used for the formation of the 6C complexes, a possible side reaction might occur:

$$[\mathrm{Fe(TPP^*)(NO)}] + 2\mathrm{L} \leftrightarrow [\mathrm{Fe(TPP^*)(L)_2}] + \mathrm{NO} \qquad (3)$$

leading to the diamagnetic low-spin complexes [Fe(TPP*)$(L)_2$]. This problem has been mostly overlooked in the

(34) Neese, F. *Inorg. Chim. Acta* **2002**, *337*, 181.
(35) (a) Rose, N. J.; Drago, R. S. *J. Am. Chem. Soc.* **1959**, *81*, 6138−6141. (b) Beugelsdijk, T. J.; Drago, R. S. *J. Am. Chem. Soc.* **1975**, *97*, 6466−6472. (c) Collman, J. P.; Brauman, J. I.; Doxsee, K. M.; Halbert, T. R.; Hayes, S. E.; Suslick, K. S. *J. Am. Chem. Soc.* **1978**, *100*, 2761−2766.
(36) $c(\mathrm{B})^0$: initial concentration of the base (MI or Py). c_T: total concentration of porphyrin complexes [$c_T = c(6C) + c(5C)$]. $\Delta\epsilon$: difference in extinction coefficients [$\Delta\epsilon = \epsilon(6C) - \epsilon(5C)$]. ΔE: change in absorbance at a specific wavelength relative to the initial absorbance ($\Delta E = E - E°$).
(37) (a) Choi, I.-K.; Ryan, M. D. *Inorg. Chim. Acta* **1988**, *153*, 25−30. (b) Liu, Y.; DeSilva, C.; Ryan, M. D. *Inorg. Chim. Acta* **1997**, *258*, 247−255.
(38) In this respect, it is interesting to note that NO behaves like a normal N-donor ligand in these ligand-binding experiments.

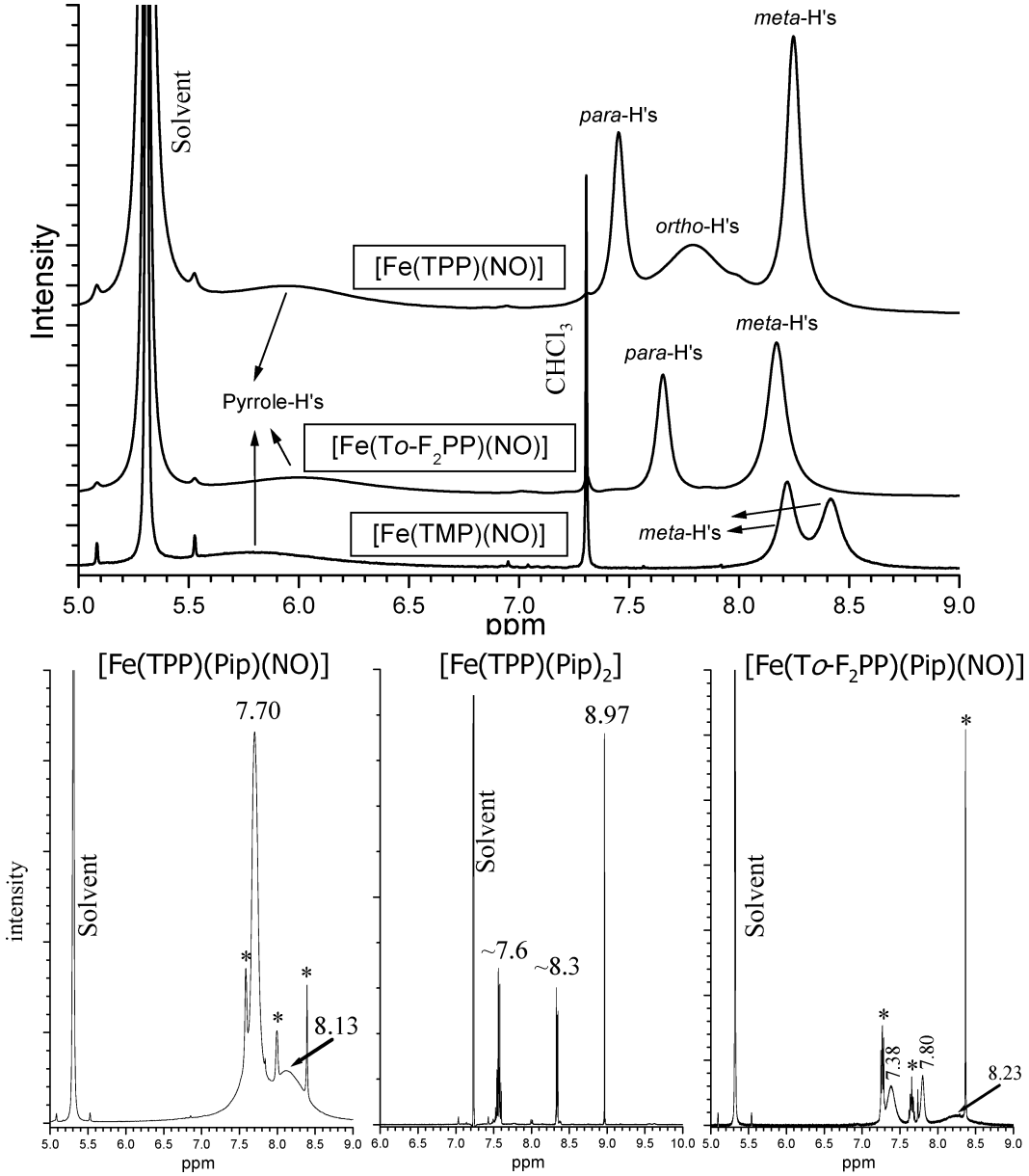

Figure 2. Top panel: ^{1}H NMR spectra of **1** (top), **1-F** (middle), and **1-Me** (bottom) in CD_2Cl_2. Bottom panel: ^{1}H NMR spectra of [Fe(TPP)(Pip)(NO)] (left), [Fe(TPP)(Pip)$_2$] (middle), and [Fe(T*o*-F$_2$PP)(Pip)(NO)] (right). The spectra of the NO complexes were obtained from solutions that contain ~15% piperidine-d_{11} (Pip). Signals marked with asterisks in these spectra belong to the corresponding [Fe(TPP*)(Pip)$_2$] complex.

literature for two reasons. First, the electronic absorption spectra of [Fe(TPP*)(L)(NO)] and [Fe(TPP*)(L)$_2$] (cf. ref 39) are usually very similar. Solution EPR[16] and IR[42a] measurements clearly show that [Fe(TPP*)(L)(NO)] is formed upon the addition of base to [Fe(TPP*)(NO)], but [Fe(TPP*)(L)$_2$] is not detected in these experiments because it is EPR-silent and does not have characteristic IR bands. Denitrosylation of **1** in the presence of Py was first observed by Lançon and Kadish.[40a] In later studies, Bohle and Hung reported rate constants for the dissociation of NO from [Fe(TPP*)(NO)] upon the addition of Py using UV−vis absorption measurements.[40b] From these data, it was concluded that denitrosylation is highly dependent on the nature of the porphyrin ligand. We found that ^{1}H NMR spectroscopy is a very useful tool to monitor the formation of even small amounts of [Fe(TPP*)(L)$_2$] in solution.

Figure 2 (top panel) shows the ^{1}H NMR spectra of the starting compounds **1**, **1-Me**, and **1-F**. The obtained signals are very broad because of the paramagnetic nature of these complexes. For compound **1**, four different signals are

(39) Safo, M. K.; Scheidt, W. R.; Gupta, G. P. *Inorg. Chem.* **1990**, *29*, 626−633.
(40) (a) Lançon, D.; Kadish, K. M. *J. Am. Chem. Soc.* **1983**, *105*, 5610−5617. (b) Bohle, D. S.; Hung, C.-H. *J. Am. Chem. Soc.* **1995**, *117*, 9584−9585.
(41) (a) Rai, B. K.; Durbin, S. M.; Prohofsky, E. W.; Sage, J. T.; Wyllie, G. R. A.; Scheidt, W. R.; Sturhahn, W.; Alp, E. E. *Biophys. J.* **2002**, *82*, 2951−2963. (b) Sage, J. T.; Paxson, C.; Wyllie, G. R. A.; Sturhahn, W.; Durbin, S. M.; Champion, P. M.; Alp, E. E.; Scheidt, W. R. *J. Phys.: Condens. Matter* **2001**, *13*, 7707−7722. (c) Leu, B. M.; Zgierski, M. Z.; Wyllie, G. R. A.; Scheidt, W. R.; Sturhahn, W.; Alp, E. E.; Durbin, S. M.; Sage, J. T. *J. Am. Chem. Soc.* **2004**, *126*, 4211−4227.
(42) (a) Yoshimura, T. *Bull. Chem. Soc. Jpn.* **1991**, *64*, 2819−2828. (b) Vogel, K. M.; Kozlowski, P. M.; Zgierski, M. Z.; Spiro, T. G. *J. Am. Chem. Soc.* **1999**, *121*, 9915−9921.

Table 3. Experimental ^{1}H NMR Shifts [ppm] of [Fe(TPP*)(NO)] and [Fe(TPP*)(Pip)(NO)] Measured against Tetramethylsilane and Assignments

		phenyl		
complex	pyrrole	ortho	meta	para
[Fe(TPP)(NO)] (**1**)	5.95	7.79	8.25	7.45
[Fe(T*o*-F_2PP)(NO)] (**1-F**)	6.00		8.17	7.65
[Fe(TMP)(NO)] (**1-Me**)	5.79		8.42/8.22	
[Fe(TPP)(Pip)(NO)]	8.13		7.70	
[Fe(T*o*-F_2PP)(Pip)(NO)]	8.23		7.38	7.80
[Fe(TMP)(Pip)(NO)]	?[a]		7.35	

[a] The signal becomes very broad and, hence, cannot be identified from the spectra with certainty.

observed at 5.95, 7.45, 7.79, and 8.25 ppm, which belong to the pyrrole hydrogens of the porphyrin core and the hydrogens in the ortho, meta, and para positions of the phenyl rings (cf. Table 3). The two signals at 5.95 and 7.79 ppm are very broad and, hence, must belong to hydrogens that are exposed to the paramagnetic center. These signals are therefore assigned as the pyrrole and *o*-phenyl hydrogens. In compound **1-F**, the ortho positions are substituted with fluorine. Hence, the ^{1}H NMR spectrum of this compound should be lacking one of the four signals observed for **1**. A comparison of the spectra in Figure 2 shows that the peak around 7.79 ppm in **1** is missing in the spectrum of **1-F**. Hence, this peak can be attributed to the *o*-phenyl hydrogens, whereas the feature at 5.95 ppm must then belong to the pyrrole hydrogens. The remaining two signals at 7.45 and 8.25 ppm can be assigned by comparison with **1-Me** (cf. Table 3), where both the ortho and para positions of the phenyl rings are substituted with methyl groups. In the titration experiments, piperidine-d_{11} (Pip) was then sequentially added to the [Fe(TPP*)(NO)] solutions, and the formation of the 6C complexes [Fe(TPP*)(Pip)(NO)] was monitored by ^{1}H NMR. Figure S6 in the Supporting Information shows the corresponding experiment performed for **1**. As one can see, a clean conversion of the 5C complex to the 6C complex is observed. The final spectrum obtained for [Fe(TPP)(Pip)(NO)] in this experiment is also shown in the bottom panel of Figure 2. In this case, the ^{1}H NMR spectrum only shows two peaks at 7.70 and 8.13 ppm. These can be traced back to the corresponding signals of the 5C complex **1**, as shown in Figure S6 in the Supporting Information. From these data, the broad signal at 8.13 ppm corresponds to the peaks at 5.95 and 7.79 ppm in **1** and is therefore assigned to the pyrrole and *o*-phenyl hydrogens. On the other hand, the peak at 7.79 ppm corresponds to both the *m*- and *p*-phenyl hydrogens, which coincide in the spectrum of [Fe(TPP)(Pip)(NO)]. In addition, three sharp peaks are observed in the spectra, which are marked with asterisks in Figure 2, bottom left. A comparison with the spectrum of pure [Fe(TPP)(Pip)$_2$] shown in Figure 2, bottom center, shows that these signals correspond to the formation of diamagnetic [Fe(TPP)(Pip)$_2$] and, hence, loss of NO upon the addition of base to the solution of **1**. Similar denitrosylation is also observed in the corresponding experiments with **1-Me** and **1-F**. The obtained spectrum of [Fe(T*o*-F_2PP)(Pip)(NO)] is shown in Figure 2, bottom right. Importantly, the amount of diamagnetic bis-piperidine complex formed is much larger for the fluoro-substituted ligand compared to TPP. At a concentration of ~15 vol % Pip, the formation of the bis-piperidine complex [Fe(TPP*)(Pip)$_2$] increases in the order TPP (8%) < TMP (~15%) < T*o*-F_2PP (31%). Hence, *the order for the degree of denitrosylation corresponds to the order of the N-donor binding constants* described above. Whereas NO loss is only marginal for TPP, this effect is very pronounced for T*o*-F_2PP. Therefore, although the fluoro-substituted ligand T*o*-F_2PP is optimal for the binding of N-donor ligands to obtain 6C $Fe^{II}NO$ complexes, it has the severe disadvantage that denitrosylation is facilitated in this system.

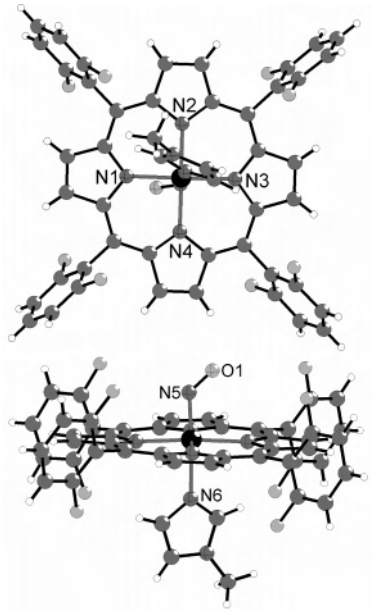

Figure 3. Top view (top) and side view (bottom) of the crystal structure of compound **2-F** with labeling. The disordered O atom is omitted for clarity.

A.3. Crystal Structure of [Fe(T*o*-F_2PP)(MI)(NO)] (2-F). To identify possible structural changes of the Fe−N−O unit induced by the stronger trans ligand binding, a crystal structure of compound **2-F** has been determined. This complex crystallizes in the monoclinic space group $P2_1/c$ with all atoms located in general positions. The iron atom is coordinated by the four porphyrin nitrogen atoms, one nitrogen atom of the MI ligand, and one nitrogen atom of nitric oxide within a slightly distorted octahedron, as shown in Figure 3. The iron atom is located in the porphyrin ring plane (deviation: 0.067 Å). The geometry of the axial N−Fe−NO unit is comparable to the general structural motif of 6C iron(II) porphyrin NO complexes with axial N-donor ligands as defined by Scheidt and co-workers.[14] Important bond distances for **2-F** are presented in Table S1 in the Supporting Information and are compared to those of the structure of **2** in Table 4. The obtained Fe−NO and N−O bond lengths of 1.75 and 1.20 Å as well as the Fe−N−O angle of 138° in **2-F** are similar to the structural data of **2**. On the other hand, the Fe−N(imidazole) bond is slightly longer in **2-F** compared to **2**. The relative orientation of the MI and NO ligands in **2-F** is almost identical with that of the room-temperature structure of **2**.[14] Hence, the crystal

Table 4. Geometric and Vibrational Properties of [Fe(TPP*)(L)(NO)] Complexes (L = MI or Missing; TPP* = Tetraphenylporphyrin-Type Ligand)

	geometric parameters [Å]					vibrational frequencies [cm^{-1}]		
molecule[a]	ΔFe−N	ΔN−O	∠Fe−N−O	ΔFe−L_{tr}	ΔFe−N_P	ν(N−O)	ν(Fe−NO)	δ(Fe−N−O)[c]
[Fe(TPP)(NO)] (**1**) cryst. struct.: ref 27[b]	1.72	1.12	149		2.00	1697	532	371 (ip)
[Fe^{II}(TPP)($^{15}N^{18}O$)]						1625	515	365 (ip)
[Fe^{II}(TMP)(NO)] (**1-Me**)						1676		
[Fe^{II}(P)(NO)], calcd, BP86/TZVP ($\tilde{\mathbf{1}}$)	1.705	1.179	146		2.019	1703	595	427 (ip), 313 (oop)
[Fe^{II}(P)(NO)], calcd, B3LYP/LanL2DZ	1.742	1.212	143		2.019	1637	507	425 (ip), 308 (oop)
[Fe(TPP)(MI)(NO)] (**2**) cryst. struct.: ref 14	1.750	1.182	138	2.173	2.008	1630	440	530 (ip), 291 (oop)
[Fe^{II}(TPP)(MI)($^{15}N^{18}O$)]						1556	431/423 (IR/R)	515 (ip), 287 (oop)
[Fe^{II}(TMP)(MI)(NO)] (**2-Me**)						1624		
[Fe(T*o*-F_2PP)(MI)(NO)] (**2-F**)	1.752	1.202	138	2.188	2.012	1624		
[Fe^{II}(P)(MI)(NO)], calcd, BP86/TZVP ($\tilde{\mathbf{2}}$)	1.734	1.186	140	2.179	2.022	1662	609	482 (ip), 317 (oop)
[Fe^{II}(P)(MI)(NO)], calcd, B3LYP/LanL2DZ	1.810	1.215	142	2.063	2.030	1611	505	430 (ip), 298 (oop)

[a] MI = 1-methylimidazole; P = porphine ligand used for calculations; values for ΔFe−N_P are averaged. [b] Highly disordered structure. [c] The δ(Fe−N−O) in-plane (ip) and out-of-plane (oop) vibrations. Note that the oop mode is strongly mixed with Fe−N_P stretches and other Fe−porphyrin vibrations and, hence, cannot be identified with one distinct normal mode.

structure does not provide any further evidence for the relatively large stability of **2-F** in solution compared to **2**.

A.4. Vibrational Properties and Assignments. The IR spectrum of [Fe(TPP)(NO)] (**1**) is shown in Figure S1 in the Supporting Information along with the corresponding $^{15}N^{18}O$-labeled data. The intense band at 1697 cm^{-1} is assigned to the N−O stretch ν(N−O) in accordance with earlier work.[16a] It shifts to 1625 cm^{-1} upon isotope substitution. In the FIR region, a second isotope-sensitive band is observed at 371 cm^{-1} that shifts to 365 cm^{-1} in the $^{15}N^{18}O$-labeled material. This feature corresponds to the in-plane (ip) Fe−N−O bending vibration δ_{ip}(Fe−N−O). From the resonance Raman spectra of **1** shown in Figure S2 in the Supporting Information (excitation at 488 nm), another isotope-sensitive band can be identified at 532 cm^{-1} that shifts to 515 cm^{-1} upon isotope labeling. This band is assigned to the Fe−N stretch ν(Fe−NO) of coordinated nitric oxide. This assignment is in agreement with the results from nuclear resonance vibrational spectroscopy (NRVS),[41] which show ν(Fe−NO) at 538 cm^{-1} for powder samples of **1**. These assignments are also in agreement with resonance Raman spectra obtained on solutions of **1**, which show ν(N−O) at 1678 cm^{-1} and ν(Fe−NO) at 524 cm^{-1}.[42] On the other hand, the assignment of δ_{ip}(Fe−N−O) to the IR band at 371 cm^{-1} is not in agreement with the NRVS study,[41a] where this mode has been assigned to a band at 470 cm^{-1}. However, no strong evidence is presented for this assignment, which is only based on the experimental result that the 470 cm^{-1} feature has an in-plane Fe displacement. Table 4 gives a compilation of the vibrational assignments presented here, which are based on actual isotope shifts coupled to a NCA. From DFT, the calculated N−O stretch for model $\tilde{\mathbf{1}}$ at 1703 cm^{-1} is in very good agreement with experiment. The in-plane bend δ_{ip}(Fe−N−O) and especially the Fe−NO stretch, on the other hand, are predicted at 427 and 595 cm^{-1}, respectively, and, hence, are obtained too high in energy in the DFT calculations (cf. Table 4).

The IR spectrum of the 6C complex [Fe(TPP)(MI)(NO)] (**2**) is shown in Figure S3 in the Supporting Information. In this case, the N−O stretch is found at 1630 cm^{-1}, which shifts to 1556 cm^{-1} upon isotope labeling. This is in agreement with earlier IR results.[11b] An additional isotope-sensitive band is observed at 440 cm^{-1} that is found at 431 cm^{-1} in the isotope-substituted material. Figure S4 in the Supporting Information shows the resonance Raman spectra of **2** excited at 488 nm. Weak isotope-sensitive peaks are found at 530 and 440 cm^{-1} that shift to 515 and 423 cm^{-1}, respectively, in the $^{15}N^{18}O$ compound. These two features at 530 cm^{-1} (from Raman) and at 440 cm^{-1} (from Raman and IR) belong to the Fe−NO stretch and the ip Fe−N−O bend. However, the detailed assignments of these vibrations are not clear because of strong mode mixing. This is evident from the fact that *both* ν(Fe−NO) and δ_{ip}(Fe−N−O) are observed in the Raman spectra of **2**, which is not the case for **1**. From DFT, the calculated ν(N−O) shows very good agreement with experiment, whereas larger deviations are observed for δ_{ip}(Fe−N−O) and ν(Fe−NO) (cf. Table 4). In agreement with experiment, the calculations predict strong mixing between these latter modes, where the feature at higher energy (609 cm^{-1}) has more Fe−NO stretching and the one at lower energy (482 cm^{-1}) has more Fe−N−O bending character in the DFT calculations.

A.5. Quantum-Chemistry-Centered Normal-Coordinate Analysis (QCC-NCA). The vibrational assignments presented above are further investigated using NCA. Because of the large sizes of the molecules **1** and **2**, the best approach for NCA is to generate an initial force field from quantum-chemical calculations. To obtain a reasonable description of the Fe−NO subunits in **1** and **2**, the TPP rings can be simplified to the porphine ligand "P" (cf. Figure 4).[41c] The calculated force fields of models $\tilde{\mathbf{1}}$ and $\tilde{\mathbf{2}}$ are therefore used for NCA without further simplification following the QCC-NCA approach (see the Experimental Section). Masses of 77 are used for the meso hydrogen atoms to better represent

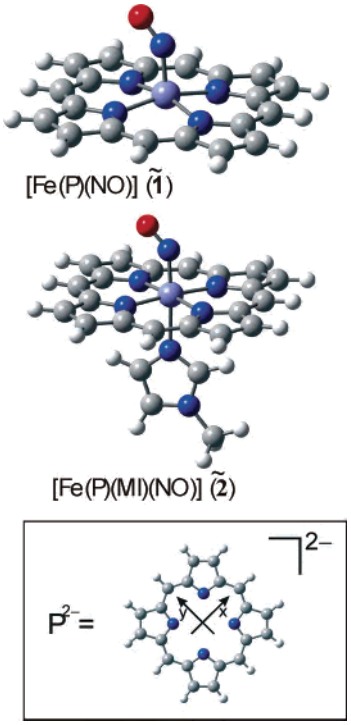

Figure 4. Figures of the fully optimized structures of $\tilde{\mathbf{1}}$ and $\tilde{\mathbf{2}}$ obtained with BP86/TZVP. Structural parameters are given in Table 4.

Table 5. Comparison of Experimental and QCC-NCA Vibrational Frequencies [cm^{-1}] and of QCC-NCA and Calculated (DFT) Force Constants [mdyn/Å]

	exptl		QCC-NCA		force constants *f*	
mode	nai[a]	$^{15}N^{18}O$	nai[a]	$^{15}N^{18}O$	QCC-NCA	calcd[b]
			[Fe(TPP)(NO)] (**1**)			
ν(N−O)	1697[c]	1625	1698	1624	12.530	12.709
ν(Fe−NO)	532	515	531	517	2.975	3.619
δ_{ip}(Fe−N−O)	371	365	371	365	0.336	0.415
			[Fe(TPP)(MI)(NO)] (**2**)			
ν(N−O)	1630	1556	1629	1557	11.550	12.224
δ_{ip}(Fe−N−O)/	530	515	529	517	0.539	0.680
ν(Fe−NO)	440	431/(423)	440	431	2.548	3.257
δ_{oop}(Fe−N−O)	291	287	(332)[d]	(328)[d]		

[a] nai = natural abundance isotopes. [b] Calculated with BP86/TZVP; see the Experimental Section. [c] Using a value of ν(NO) = 1678 cm^{-1} measured in solution,[42] force constants of 12.190 mdyn/Å for N−O and 2.985 mdyn/Å for Fe−NO are obtained. [d] Because of the fact that the oop bend shows strong mixing with porphyrin modes, a reasonable NCA fit of this mode could not be achieved within the chosen model. Hence, the energies listed are those obtained from NCA without further adjustment of force constants. Free NO: ν(N−O) = 1876 cm^{-1}; f_{N-O} = 15.49 mdyn/Å. NO^+: ν(N−O) = 2387 cm^{-1} in $(NO^+)(BF_4^-)$; f_{N-O} = 25.07 mdyn/Å. [67]

the phenyl groups of TPP. The results of this treatment are presented in Table 5, which show excellent agreement with experiment for both **1** and **2**. This further supports the vibrational assignments presented above. For complex **1**, the observed mixing between ν(Fe−NO) and δ_{ip}(Fe−N−O) is quite small. The mode at 532 cm^{-1} is a pure Fe−NO stretching vibration with 88% ν(Fe−NO). The mode at 371 cm^{-1} has 55% in-plane (ip) Fe−N−O bending character [39% contribution of δ_{ip}(Fe−N−O) and 16% from N−Fe−N(O) bends]. The ip bend δ_{ip}(Fe−N−O) is also mixed with porphyrin core modes and, hence, shows small contributions to several other vibrations. This situation changes dramatically for complex **2**. Here, ν(Fe−NO) and δ_{ip}(Fe−N−O) are closer in energy, which leads to an almost equal mixing of these vibrations. Hence, the mode at 530 cm^{-1} has 33% ν(Fe−NO) and 30% δ_{ip}(Fe−N−O) character. The mode at 440 cm^{-1}, on the other hand, has 47% ν(Fe−NO), 11% δ_{ip}(Fe−N−O), and 9% δ(N−Fe−N) bending character. Hence, the distinction between ν(Fe−NO) and δ_{ip}(Fe−N−O) is practically lost. Because of the fact that the 440 cm^{-1} mode has more Fe−NO stretching character, it is designated as ν(Fe−NO) in Table 4.

For complex **1**, N−O and Fe−NO force constants of 12.53 and 2.98 mdyn/Å are obtained as shown in Table 5. The Fe−NO force constant of about 3 mdyn/Å corresponds to a very strong bond in agreement with the very large experimental NO binding constants for iron(II) porphyrins.[43] In comparison, both the N−O and Fe−NO force constants of 11.55 and 2.55 mdyn/Å, respectively, are distinctively *smaller* for **2**. Because the Fe−NO interaction is mediated by π^* orbitals of NO in these complexes, these findings can only be explained if complex **1** has a stronger Fe−NO σ bond. Increased donation from a NO antibonding (π^*) orbital in the case of **1** then leads to a strengthening of both the Fe−NO and N−O bonds relative to **2**, in agreement with the trend in force constants. The weaker N−O bond in **2** could also be explained with a larger amount of back-donation from iron(II) to the π^* orbitals of NO. However, this would lead to an inverse correlation of the Fe−NO and N−O bond strengths, which is not the case experimentally. Hence, *complexes **1** and **2** differ significantly in the strength of the Fe−NO σ interaction*. The calculated force constants from DFT show, in general, good agreement with the NCA result, as presented in Table 5. The only exceptions in this respect are the Fe−NO force constants, which are calculated distinctively too large (vide infra). On the basis of their NRVS data, Rai et al. have also performed an NCA for the low-energy modes of **1** including ν(Fe−NO) and δ_{ip}(Fe−N−O).[41a] The obtained force constants of 2.66 mdyn/Å for Fe−NO and 0.30 mdyn for Fe−N−O compare well with the results presented here. The lower value for the Fe−NO force constant is due to their fit of δ_{ip}(Fe−N−O) to a mode at 470 cm^{-1} (vide supra), which differs from our results. However, because our analysis is supported by the experimentally determined isotope shifts and the good quality of the NCA fit of these data, we are confident that we have arrived at a more consistent assignment of the vibrational data of the Fe−N−O subunit of **1** and that the observed tendencies in the N−O and Fe−NO force constants for **1** and **2** are valid.

B. Electronic Structure of Iron(II) Porphyrin NO Adducts and Assignments of Optical Spectra. The complete bonding scheme of the six-coordinate (6C) complex [Fe(TPP)(MI)(NO)] (**2**) obtained from DFT calculations is analyzed in detail. This electronic structure is then compared to that of the corresponding five-coordinate (5C) species [Fe(TPP)(NO)] (**1**) in relation to the experimental results presented above. Calculated EPR and Mössbauer hyperfine

(43) Ford, P. C.; Laverman, L. E. *Coord. Chem. Rev.* **2005**, *249*, 391−403.

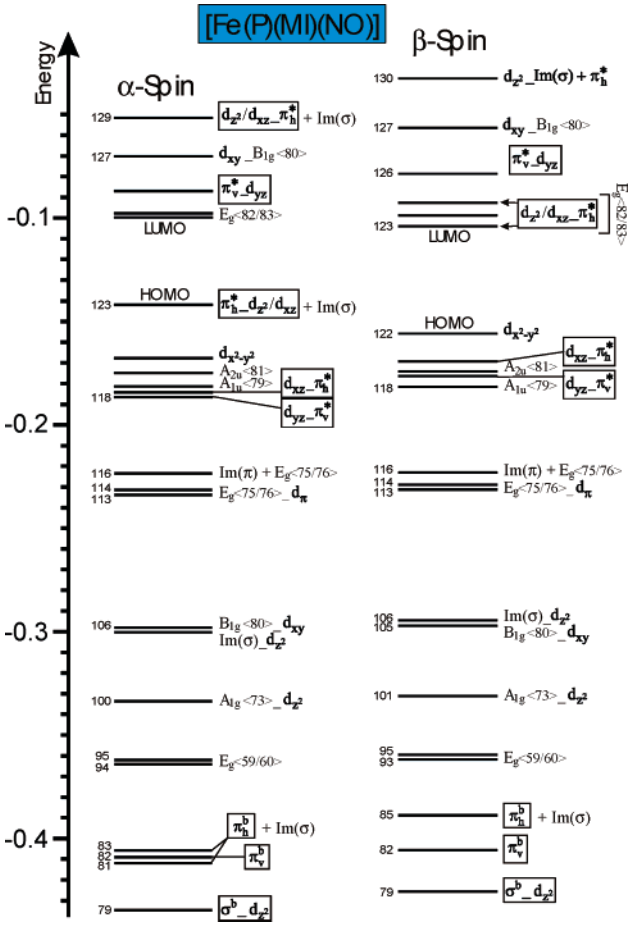

Figure 5. MO diagram of [Fe(P)(MI)(NO)] ($\tilde{\mathbf{2}}$) calculated with BP86/TZVP. The applied coordinate system is shown in Figure 4. A_{1u}, A_{2u}, E_g, etc., correspond to porphyrin orbitals, as shown in Figure S7 in the Supporting Information. Ligand orbitals of NO are labeled π_v^* (v = vertical; orthogonal to the Fe−N−O plane) and π_h^* (h = horizontal; located in the Fe−N−O plane) and are shown in Figure S8 in the Supporting Information. The nomenclature *a_b* indicates that orbital *a* interacts with *b* and that *a* has a larger contribution to the resulting MO.

parameters are also discussed. Finally, the MCD spectra of complexes **1** and **2** are assigned.

B.1. Bonding Description of Complex 2 and Comparison to 1. To analyze the electronic structures of 5C and 6C iron(II) porphyrin NO complexes, the model systems [Fe(P)(NO)] ($\tilde{\mathbf{1}}$) and [Fe(P)(MI)(NO)] ($\tilde{\mathbf{2}}$) have been applied, as shown in Figure 4. Geometry optimization was then performed using B3LYP/LanL2DZ and BP86/TZVP. Table 4 shows that, in the case of **1**, both methods lead to very good agreement with the experimental structure. However, for the 6C complex **2**, the B3LYP geometry is clearly of a lower quality, whereas BP86 again shows excellent agreement with experiment. Hence, the analysis of the electronic structures of **1** and **2** is based on the fully optimized structures $\tilde{\mathbf{1}}$ and $\tilde{\mathbf{2}}$ from BP86/TZVP. Figure 5 presents the corresponding molecular orbital (MO) diagram for model $\tilde{\mathbf{2}}$. Charge distributions are given in Table S2 in the Supporting Information. Figure 4 shows the applied coordinate system used in the following discussion. The *z* axis is roughly oriented along the N(imidazole)−Fe−N(O) axis. In complex **2**, iron is in the +II oxidation state and is low-spin (as is evident from EPR), which leads to a $[d_{xz}, d_{yz}, d_{x^2-y^2}]^6 \approx [t_2]^6$ electron configuration of the metal.[44] Bonding to the porphyrin ligand is mostly mediated by the frontier orbitals of this ligand. The MO diagram of free porphine^{2-} used as a model for TPP in the calculations is shown in Figure S7 in the Supporting Information. The lowest unoccupied MO (LUMO) of the porphine ligand corresponds to a pair of degenerate π^* orbitals of E_g symmetry, labeled $E_g\langle 82/83\rangle$ in Figure 5.[45] These undergo a very weak back-bonding interaction with the d_{xz} and d_{yz} orbitals of iron (1−3% d orbital admixture). The highest occupied π orbitals are of A_{2u} and A_{1u} symmetry and are practically nonbonding to the d orbitals. The iron−porphine σ bond is mediated by the in-plane (ip) B_{1g} orbital and the unoccupied d_{xy} orbital of iron. The MO diagram of free nitric oxide is presented in Figure S8 in the Supporting Information. This molecule is a radical ($S = {}^1/_2$ ground state), with the unpaired electron being located in the singly occupied π^* orbitals. Because complex **2** has a total spin of $S = {}^1/_2$, the spin-unrestricted scheme has to be applied, which distinguishes between majority (α) and minority (β) spin orbitals. The unpaired electron of NO occupies the orbital α-π_h^* (h = horizontal), which is located in the Fe−N−O plane. Because the t_2 functions of Fe^{II} are fully occupied, σ donation from α-π_h^* to the metal is only possible into the d_{z^2} orbital. The corresponding bonding combination, π_h^*_d_{z^2}/d_{xz} ($\alpha\langle 123\rangle$), is the highest occupied MO (HOMO) of $\tilde{\mathbf{2}}$ (cf. the contour plot in Figure 6). It has about 43% π_h^* and 42% mixed d_{z^2}/d_{xz} contribution, which corresponds to a strong interaction. Note that the interaction of π_h^* and d_{xz} does not contribute to bonding because both orbitals are occupied. The second α-π^* orbital of NO, labeled π_v^* (v = vertical), is unoccupied and oriented perpendicular to the Fe−N−O plane. It forms a medium-strong π back-bond with d_{yz} of iron. The corresponding antibonding combination, π_v^*_d_{yz} ($\alpha\langle 126\rangle$), consists of 71% π_v^* with 24% d_{yz} admixture, as shown in Table S2 in the Supporting Information and Figure 6. An additional small contribution to the Fe−NO bond is only found for the weakly N−O σ-bonding orbital σ^b (cf. Figure S8 in the Supporting Information; 7% d_{z^2} admixture). In the spin-unrestricted scheme, both β-π_h^* and β-π_v^* of NO are unoccupied and undergo additional π-back-bonding interactions with iron (cf. Figure 6). The corresponding bonding combinations, d_{xz}_π_h^* ($\beta\langle 121\rangle$) and d_{yz}_π_v^* ($\beta\langle 119\rangle$), have about 50% metal d and about 20% π^* contribution (cf. Table S2 in the Supporting Information). The antibonding combination, π_v^*_d_{yz} ($\beta\langle 126\rangle$), consists of 67% π_v^* and 27% d_{yz}, which is comparable to α spin. In summary, NO acts as a medium-strong σ-donor and π-acceptor ligand in $\tilde{\mathbf{2}}$.

The interesting question is then, how does this electronic structure change when going from 6C complex **2** to 5C complex **1**? The experimentally determined Fe−NO force

(44) In the applied coordinate system (cf. Figure 4), the $d_{x^2-y^2}$ orbital can formally be identified with one of the "t_2" orbitals, whereas d_{xy} undergoes a σ bond with the porphyrin and can therefore be classified as an "e" orbital.

(45) For the presentation of the electronic structure of $\tilde{\mathbf{2}}$ (Figures 5 and 6 and Table S2 in the Supporting Information), the MOs of the porphine^{2-} ligand are labeled as shown in Figure S7 in the Supporting Information. For example, the HOMO of porphine^{2-} is $A_{2u}\langle 81\rangle$.

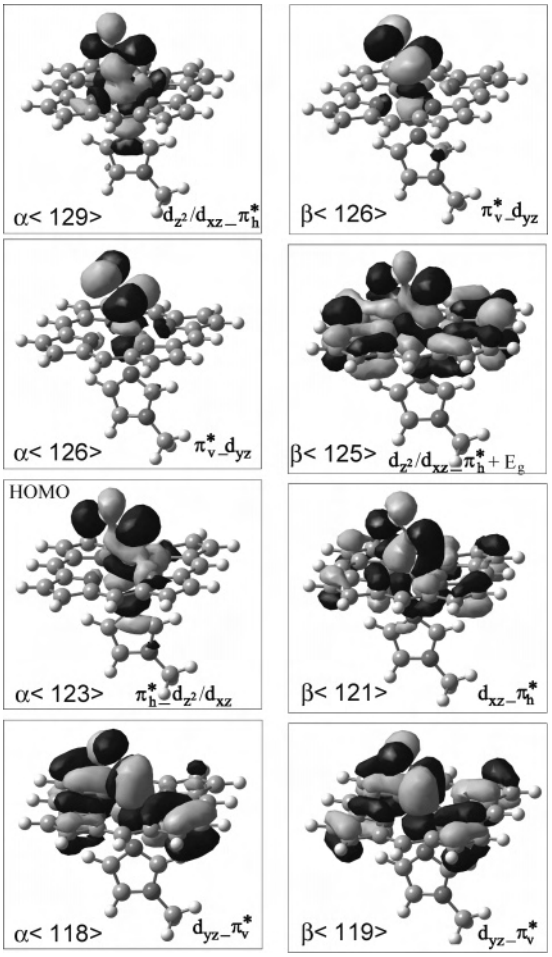

Figure 6. Contour plots of important MOs of $\tilde{\mathbf{2}}$ calculated with BP86/TZVP. For the labels, see Figure 5 and Table S2 in the Supporting Information.

constants, which are 2.98 mdyn/Å for **1** and 2.55 mdyn/Å for **2**, show that there is a significant difference in the Fe−NO bond strengths in these complexes. As shown in section A.5, this relates to differences in the Fe−NO σ bond in agreement with DFT results published in a preceding Communication,[18] which predict a stronger σ interaction in **1**.[46] This change in the Fe−NO bond strengths should be reflected by the spin densities. To calculate accurate spin densities, the B3LYP functional has to be applied because pure density functionals tend to overestimate the metal−ligand covalencies. A comparison of the calculated Fe−NO force constants from BP86 with experiment (cf. Table 5) shows that this is also the case here. Because spin polarization effects are quite small for $\tilde{\mathbf{1}}$ and $\tilde{\mathbf{2}}$,[47] the calculated spin densities roughly correspond to the shape of the singly occupied MOs (SOMOs) of $\tilde{\mathbf{1}}$ and $\tilde{\mathbf{2}}$ shown in Figure 7. The unpaired electron is mostly localized on the NO ligand (spin density: +0.8) in the 6C complex. In comparison, values

(46) The Fe−NO π back-bonds are similar for $\tilde{\mathbf{1}}$ and $\tilde{\mathbf{2}}$. Small differences are only observed for the β-MOs, where the π back-bond is slightly stronger for $\tilde{\mathbf{1}}$. For example, the antibonding combination $\pi_v^*-d_{yz}$ (β-$\langle 104\rangle$) has 57% π_v^* and 35% d_{yz} character compared to 67% π_v^* and 27% d_{yz} ($\beta\langle 126\rangle$) for $\tilde{\mathbf{2}}$. This leads to the transfer of a small additional amount of spin density from NO to iron in $\tilde{\mathbf{1}}$ relative to $\tilde{\mathbf{2}}$.

(47) Praneeth, V. K. K.; Haupt, E.; Lehnert, N. *J. Inorg. Biochem.* **2005**, *99*, 940−948.

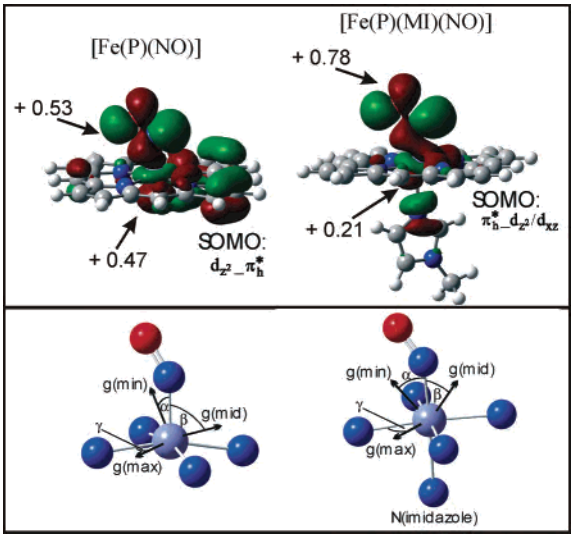

Figure 7. Top: Contour plots of the SOMOs of [Fe(P)(NO)] ($\tilde{\mathbf{1}}$) and [Fe(P)(MI)(NO)] ($\tilde{\mathbf{2}}$) calculated with B3LYP/LanL2DZ*. Calculated for the fully optimized structures obtained with BP86/TZVP. The calculated spin densities reflect the shape of the SOMO in both cases. Spin densities on Fe and NO are indicated. Bottom: calculated orientation of the principal axes of the *g* tensor relative to the molecular frame using BP86/TZVP.

of +0.5 on Fe and +0.5 on NO are obtained for $\tilde{\mathbf{1}}$, which corresponds to an increase in the Fe−NO covalency and, hence, the metal−ligand bond strength. These spin densities are also in agreement with MCD[18] and ^{1}H NMR results (see the Discussion section).

B.2. Calculation of Hyperfine Parameters of 1 and 2. The results presented above are very useful to evaluate the very different EPR spectra of 5C and 6C iron(II) porphyrin NO adducts[16] (see the Introduction). In a preceding Communication, these differences were analyzed based on calculated *g* tensors for models $\tilde{\mathbf{1}}$ and $\tilde{\mathbf{2}}$.[18] In agreement with earlier calculations,[17] it was found that the orientation of the *g* tensor in the molecular frame is different in these complexes, as shown in Figure 7. However, the question of how this relates to the electronic structure descriptions of these systems as elaborated above is still open. First, the fact that complex **2** shows smaller overall *g* shifts than **1** reflects the decreased spin density on iron in this complex.[17,48] Second, the rotation of the *g* tensor in **2** compared to **1** might relate to the change of the "magnetic orbital" of iron in these complexes. In the case of **1**, the spin density on iron is located in an orbital of mostly d_{z^2} character, which is oriented along the *z* axis. On coordination of the sixth ligand, the orbital becomes stronger mixed with d_{xz} and, hence, is rotated off the *z* axis (cf. the SOMOs in Figure 7). Presumably, the *g* tensor then follows the rotation of the spin density at the iron center.

In addition to the *g* tensor, we have also calculated the ^{14}N and ^{57}Fe hyperfine (*A*) tensors and Mössbauer parameters

(48) This is in agreement with the differences in spin density distribution for **1** and **2** as evidenced by MCD spectroscopy and the different ^{1}H NMR chemical shifts of the pyrrole hydrogens in these systems (cf. Table 3). In diamagnetic [Fe(TPP)(Pip)$_2$] (cf. Figure 2), these signals are observed at 8.97 ppm, which is close to the value of ~8.1 ppm for **2**. In contrast, these hydrogens show a stronger paramagnetic shift to 5.95 ppm in **1**. Correspondingly, the calculated spin densities on the pyrrole hydrogens are 2−4 times larger in **1** than they are in **2**.

Table 6. Comparison of Experimental and Calculated ^{14}N Hyperfine (A) Tensors of the Nitrosyl Nitrogen in **1** and **2** and Related Model Complexes[a]

molecule	^{14}N hyperfine $A[g]$ [MHz]			orientation
	$A[g(\max)]$	$A[g(\mathrm{mid})]$	$A[g(\min)]$	
[Fe(TPP)(NO)], exptl[16a]	37.1	49.7	48.7	?
[Fe(OEP)(NO)], exptl[b,16d]	40.9	49.7	42.7	g/A: 30° [c]
[Fe(P)(NO)] ($\tilde{\mathbf{1}}$), calcd	28.3	62.0	49.9	$A[g(\min)]$/Fe−N: 1° [d]
[Fe(TPP)(Pip)(NO)], exptl[16a]		60.8		?
[Fe(P)(MI)(NO)] ($\tilde{\mathbf{2}}$), calcd	15.2	84.0	13.2	$A[g(\min)]$/Fe−N: 30° [e]

[a] The values of the A tensor [MHz] are given relative to the g tensor; i.e., a given A value is paired with the g value whose principal axis is closest to the principal axis of this A. The column "orientation" then gives the relative orientation of the A tensor. [b] Single-crystal EPR data. [c] Angle between the principal axes of the g and A tensors. [d] The angle between the principal axes of $g(\min)/A[g(\min)]$ and $g(\mathrm{mid})/A[g(\mathrm{mid})]$ is about 20°; $g(\max)$ and $A[g(\max)]$ are collinear and oriented perpendicular to the Fe−N−O plane. [e] The angle between the principal axes of $g(\min)/A[g(\min)]$ and $g(\mathrm{mid})/A[g(\mathrm{mid})]$ is about 30°; $g(\max)$ and $A[g(\max)]$ are collinear and oriented perpendicular to the Fe−N−O plane.

for models $\tilde{\mathbf{1}}$ and $\tilde{\mathbf{2}}$ using the B3LYP functional. For the 5C complexes, the experimental ^{14}N hyperfine tensor is quite isotropic, with $A[g(\mathrm{mid})] \approx 50$ MHz being somewhat larger than the other two values, although the experimental results for **1** and [Fe(OEP)(NO)] are somewhat different in this respect, as shown in Table 6. From the Fe$^{\mathrm{II}}$NO adduct of hemoglobin, it is known that the hyperfine tensor becomes quite anisotropic in the case of a 6C complex (values of 29.6, 32.9, and 63.6 MHz (α subunit) and 26.9, 44.2, and 62.3 MHz (β subunit) have been determined).[49] In agreement with this, the $A[g(\mathrm{mid})]$ value of [Fe(TPP)(Pip)(NO)] has been determined from solution EPR to be 61 MHz.[16a] The general trend with the A tensor being more anisotropic for 6C compared to 5C Fe$^{\mathrm{II}}$NO complexes is reproduced well by the calculations. The calculated values of $A[g(\min)] = 49.9$ MHz for $\tilde{\mathbf{1}}$ and $A[g(\mathrm{mid})] = 84.0$ MHz for $\tilde{\mathbf{2}}$ can be directly compared to solution EPR data and show very good agreement. The other A values show some deviations (cf. Table 6), but the overall agreement between theory and experiment is satisfactory. In a recent publication, ^{14}N hyperfine couplings for a model similar to $\tilde{\mathbf{2}}$ were calculated to be 29, 31, and 74 MHz for the minimum-energy structure,[20d] which agrees with our results. Table S3 in the Supporting Information lists the calculated Mössbauer isomer shifts δ and quadrupole splittings ΔE_q for models $\tilde{\mathbf{1}}$ and $\tilde{\mathbf{2}}$ in comparison with experiment. The isomer shifts are reproduced well, indicating that the electron densities are well described by our calculations. The quadrupole splittings and the ^{57}Fe hyperfine tensor elements show noticeable deviations (cf. Table S3 in the Supporting Information). One source of the observed errors relates to the chosen basis sets for these calculations. Previous DFT work of Oldfield and co-workers using the "locally dense" basis set approach[50] on [Fe(OEP)(NO)] and model systems comparable to $\tilde{\mathbf{1}}$ and $\tilde{\mathbf{2}}$ led to quadrupole splittings that are in excellent agreement with experiment.[20c,d] Therefore, the calculation of the quadrupole and ^{57}Fe hyperfine tensors seems to require extensively large basis sets.

B.3. Assignment of the Optical Spectra. The absorption and MCD spectra of porphyrin complexes are dominated by intense $\pi \rightarrow \pi^*$ transitions of the porphyrin dianion.[21a,51] These have been analyzed in detail by Gouterman. The $A_{1u}\langle 79\rangle$, $A_{2u}\langle 81\rangle$ (HOMO) to $E_g\langle 82/83\rangle$ (LUMO) (cf. Figure S7 in the Supporting Information) transitions give rise to two excited states of E_u symmetry. These show strong configuration interaction (CI) coupling, leading to the intense Soret or B band at higher energy ($\epsilon \geq 100\,000$ M^{-1} cm^{-1}) and the Q band at lower energy, which has low to zero intensity (depending on the actual complex). The corresponding wave functions for these excited states are therefore defined as

$$|\Psi^{\mathrm{Soret}}\rangle = \frac{1}{\sqrt{2}}|\psi_1 + \psi_2\rangle \quad \text{and} \quad |\Psi^{\mathrm{Q}}\rangle = \frac{1}{\sqrt{2}}|\psi_1 - \psi_2\rangle$$

where ψ_1: $A_{1u}\langle 79\rangle \rightarrow E_g\langle 82/83\rangle$ and ψ_2: $A_{2u}\langle 81\rangle \rightarrow E_g\langle 82/83\rangle$ are the individual excited states of E_u symmetry. Because of vibronic mixing of the Q state with the Soret state, an additional quite intense band designated as Q_v is observed at about 1250 cm^{-1} to higher energy from Q.[51,52] Because complexes **1** and **2** have a low-spin d^6 configuration, the three t_2 orbitals of iron(II) (vide supra) are fully occupied and, hence, no low-energy porphyrin (π) to metal (t_2) charge-transfer transitions are possible in these cases. Therefore, the absorption spectra of complexes **1** and **2** are dominated by only two features: the intense Soret band at around 400 nm and the Q_v band at about 540 nm.[51] Figures 8 and 9 show the absorption and MCD **C**-term spectra of complexes **1** and **2**, respectively, which allow for the identification of 10 electronic transitions below 30 000 cm^{-1}. Table 7 summarizes the band positions obtained from correlated Gaussian fits of these data (included in Figures 8 and 9). Because the spectra were measured under different experimental conditions, small differences in the band positions were tolerated in the fit. To assign the electronic spectra of complexes **1** and **2**, TD-DFT calculations on the B3LYP level have been performed. Using the porphine approximation, the calculated Soret band positions of 28 500 cm^{-1} for $\tilde{\mathbf{1}}$ and 26 670 cm^{-1} for $\tilde{\mathbf{2}}$ only show poor agreement with experiment, as shown

(49) Utterback, S. G.; Doetschman, D. C.; Szumowski, J.; Rizos, A. K. *J. Chem. Phys.* **1983**, *78*, 5874−5880.
(50) Chestnut, D. B.; Moore, K. D. *J. Comput. Chem.* **1989**, *10*, 648−659.
(51) Gouterman, M. Optical Spectra and Electronic Structure of Porphyrins and Related Rings. In *The Porphyrins*; Dolphin, D., Ed.; Academic Press: New York, 1978; Vol. III.
(52) (a) Spiro, T. G.; Strekas, T. C. *Proc. Natl. Acad. Sci. U.S.A.* **1972**, *69*, 2622−2626. (b) Spiro, T. G. In *Iron Porphyrins*; Lever, A. B. P., Gray, H. B., Eds.; Addison-Wesley: Reading, MA, 1983; Part 2. (c) Egawa, T.; Suzuki, N.; Dokoh, T.; Higuchi, T.; Shimada, H.; Kitagawa, T.; Ishimura, Y. *J. Phys. Chem. A* **2004**, *108*, 568−577. (d) Paulat, F.; Praneeth, V. K. K.; Näther, C.; Lehnert, N. *Inorg. Chem.* **2006**, in press.

Table 7. Correlated Fit of the UV−Vis Absorption and MCD **C**-Term Spectra of **1** and **2**[a]

	[Fe(TPP)(NO)] (**1**)				[Fe(TPP)(MI)(NO)] (**2**)			
		UV−vis				UV−vis		
no.	MCD **C** term	position	ϵ[b]	assignment[c]	MCD **C** term	position	ϵ[b]	assignment[c]
1	15268	(15200)	266	$Q^{(1)}$				
2	16451	16298	2126	$Q_v^{(1)}$	16551	16412	3807	$Q^{(1)}$
3	17028	(17042)	410	$Q^{(2)}$	17239	17166	3358	$Q^{(2)}$
3a					17894	17742	6954	$Q_v^{(1)}$
4	18252	18401	8098	$Q_v^{(2)}$	18275	18554	14180	$Q_v^{(2)}$
5	20311	20241	4893	$\pi \rightarrow \pi^{*(3)}$, $CT^{(1)}$	(19935)	19955	6052	$CT^{(1)}$, $\pi \rightarrow \pi^{*(3)}$
6	21858	21499	9858	$CT^{(1)}$, $\pi \rightarrow \pi^{*(1)}$, Soret	21880	21644	9388	$CT^{(1)}$, $\pi \rightarrow \pi^{*(1)}$, Soret
6a					22867	(22331)	15185	$Soret^{(1)}$
7	23583	23436	35030	$Soret^{(1)}$	**23507**	**23470**	**146880**	**$Soret^{(2)}$**
8	**24530**	**24840**	**82184**	**$Soret^{(2)}$**	24166	24495	44087	$Soret^{(3)}$
9	25624			$\pi \rightarrow \pi^{*(3)}$, $CT^{(2)}$, Soret	25127	25541	(14719)	$CT^{(1)}$?, Soret
10	26869	26969	(17896)	$CT^{(2)}$				
11					28238	28180		$\pi \rightarrow \pi^{*(1,3)}$
12					30894	30971		$\pi \rightarrow \pi^{*(1,3)}$

[a] The parentheses are used when a band position cannot be exactly determined from the data. For the fit, the *minimum number* of Gaussians has been used. If, for example, a band can be identified from the MCD spectrum but no corresponding band is necessary to fit the absorption spectrum, then the absorption data are not fit with this feature. Hence, in very few cases, bands appear in the correlated fit of the MCD spectra, but not in the fit of the absorption spectra (and vice versa). [b] ϵ is given in M^{-1} cm^{-1}. [c] Electronic transitions (cf. Figures 5 and S7 in the Supporting Information): CT = charge transfer; $\pi \rightarrow \pi^*$ = porphyrin $\pi \rightarrow \pi^*$ transition; see text.

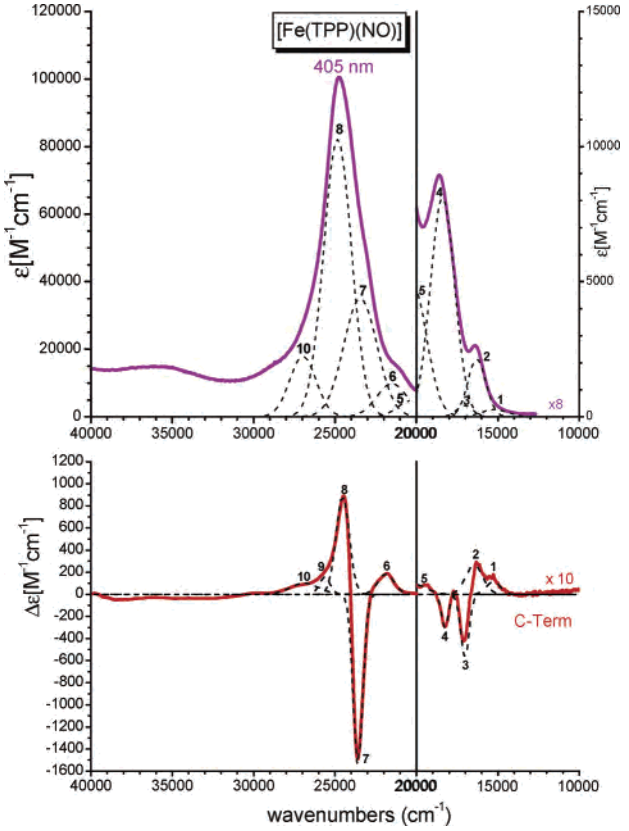

Figure 8. Electronic spectra of [Fe(TPP)(NO)] (**1**). Top: UV−vis spectrum measured in CH_2Cl_2 at room temperature. Bottom: MCD **C**-term spectrum measured in propionitrile/butyronitrile (1:1) at 2 K. The dashed lines represent a correlated fit of these data (cf. Table 7).

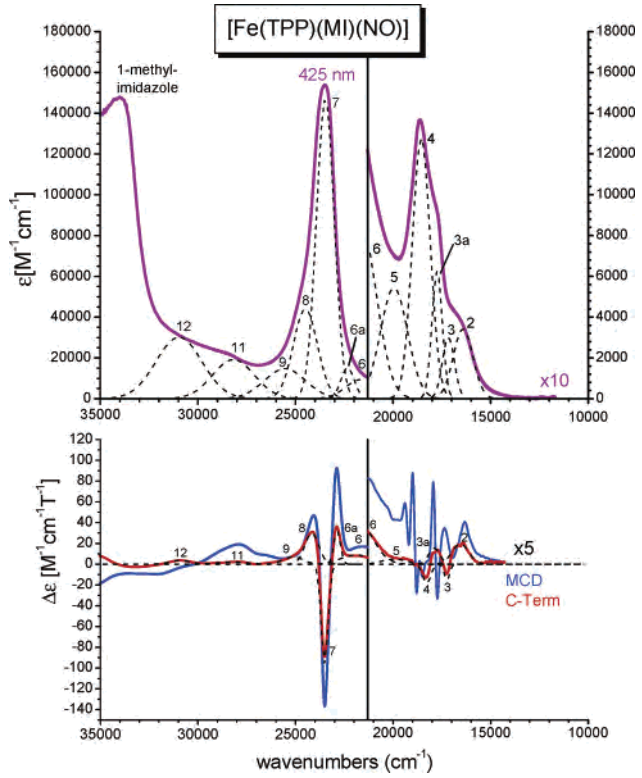

Figure 9. Electronic spectra of [Fe(TPP)(MI)(NO)] (**2**). Top: UV−vis spectrum measured in CH_2Cl_2 at room temperature. Bottom: MCD spectra measured in propionitrile/butyronitrile (1:1) at 5 K. The dashed lines represent a correlated fit of the UV−vis absorption and the MCD **C**-term data (cf. Table 7).

in Table 8. In addition, the shift of the Soret band from **1** to **2** is calculated to be 1830 cm^{-1}, which is too large. Using semiempirical INDO/S-CI calculations on $\tilde{\mathbf{1}}$ and $\tilde{\mathbf{2}}$ leads to some improvement of the theoretical Soret band positions, but the deviation from experiment is still unsatisfactory. This result is not surprising considering that the Soret and Q bands actually correspond to porphyrin $\pi \rightarrow \pi^*$ transitions. Hence, neglect of the phenyl substituents of TPP introduces a significant error to the geometric and electronic structures of the porphyrin ring. We then tried to perform TD-DFT calculations using the complete TPP ligand by applying the crystal structures of **1** and **2**,[14,27,53] but convergency of these calculations could not be achieved. Therefore, the INDO/S-CI method was used again, and this leads to very good agreement between the experimental and calculated Soret band positions, but deviations are also observed, as shown in Table 8. Therefore, because of the fact that none of the

Table 8. Calculated Q and Soret Band Energies Compared to Experiment

model/method	transition energy Q	transition energy Soret	Δ(5C−6C) Soret
[Fe(TPP)(NO)]/exp	**15268/17028**[a]	**24530**[a]	
[Fe(P)(NO)]/TD-DFT	19370	28500	
[Fe(P)(NO)]/INDO/S-CI	14960	26420	
[Fe(TPP)(NO)]/INDO/S-CI	15470	24740	
[Fe(TPP)(MI)(NO)]/exp	**16551/17239**[a]	**23507**[a]	1023
[Fe(P)(MI)(NO)]/TD-DFT	19090	26670	1830
[Fe(P)(MI)(NO)]/INDO/S-CI	14610	25730	690
[Fe(TPP)(MI)(NO)]/INDO/S-CI	14080	24260	480

[a] From MCD; cf. Table 7.

excited-state calculations leads to an overall satisfactory agreement with experiment, the INDO/S-CI calculations on the entire complexes will serve as a basis for an only semiquantitative interpretation of the optical spectra of **1** and **2**.

Assignment of the Soret Region. Because of the presence of the phenyl substituents, the effective symmetry of the TPP ligand in complexes **1** and **2** is lower than D_{4h}. Hence, the 2-fold degeneracy of the LUMO $E_g\langle 82/83\rangle$ is lifted, which leads to a splitting of the individual excited states ψ_1 and ψ_2 into two components:

$$\psi_{1a}\text{: } A_{1u}\langle 79\rangle \rightarrow E_g^{(1)} \qquad \psi_{2a}\text{: } A_{2u}\langle 81\rangle \rightarrow E_g^{(1)}$$

$$\psi_{1b}\text{: } A_{1u}\langle 79\rangle \rightarrow E_g^{(2)} \qquad \psi_{2b}\text{: } A_{2u}\langle 81\rangle \rightarrow E_g^{(2)}$$

In the simplest approximation used in the following, the energetically split LUMO $E_g\langle 82/83\rangle$ is considered but, otherwise, an effective D_{4h} symmetry is assumed. CI coupling of the individual transitions then leads via cross-coupling to the Soret and Q states:

$$|\Psi_1^{\text{Soret}}\rangle = \frac{1}{\sqrt{2}}|\psi_{1a} + \psi_{2b}\rangle$$

$$|\Psi_2^{\text{Soret}}\rangle = \frac{1}{\sqrt{2}}|\psi_{2a} + \psi_{1b}\rangle$$

$$|\Psi_1^{\text{Q}}\rangle = \frac{1}{\sqrt{2}}|\psi_{1a} - \psi_{2b}\rangle$$

$$|\Psi_2^{\text{Q}}\rangle = \frac{1}{\sqrt{2}}|\psi_{2a} - \psi_{1b}\rangle$$

As shown by Neese and Solomon, the MCD **C**-term intensity C_0 for an $S = {}^1/_2$ (orbitally nondegenerate) ground state is defined by[21c]

$$C_0 = -\frac{1}{6}\sum_{uvw}\epsilon_{uvw}g_w\sum_{K\neq A,J}\{\Delta_{KJ}^{-1}(\vec{D}_u^{KA}\times\vec{D}_v^{AJ})\cdot\bar{L}_w^{KJ} + \Delta_{KA}^{-1}(\vec{D}_u^{AJ}\times\vec{D}_v^{JK})\cdot\bar{L}_w^{KA}\} \quad (4)$$

for a transition from the ground state $|A\rangle$ to the excited state $|J\rangle$, where $|K\rangle$ is an intermediate state. This expression can be used to derive an equation for the **C**-term intensity of the Soret band. In this case, the two Soret excited states Ψ_1^{Soret} and Ψ_2^{Soret} represent a couple of energetically close excited states with orthogonal transition dipole moments. Excited-state spin−orbit coupling (SOC) between these states leads to the following expression for the **C**-term intensity as derived in the Supporting Information:

$$I^{\text{MCD}} \sim -\frac{c^2\zeta^{\text{Fe}}}{\Delta_{\text{Soret}}}(\vec{D}_u^{\text{Soret(1)}}\times\vec{D}_v^{\text{Soret(2)}}) \quad (8)$$

The corresponding SOC matrix element is proportional to $c^2\zeta^{\text{Fe}}$, where c represents the coefficient of d orbital admixture to the porphyrin E_g orbitals (<5% contribution; see the Supporting Information). Hence, the SOC matrix element is quite small because of the very small coefficients, but this is compensated for by the large transition dipole moments of the Soret band. If one alternatively considers the transition to Ψ_1^{Soret} as $|J\rangle$ and Ψ_2^{Soret} as intermediate state $|K\rangle$, the same expression for the **C**-term intensity in eq 8 is obtained, but because of the sign change in the denominator Δ^{-1} that occurs when $|K\rangle$ and $|J\rangle$ are exchanged, the resulting **C**-term signal changes its sign. Hence, this mechanism gives rise to a so-called pseudo-**A** term in the MCD spectrum,[21c] where two adjacent bands are observed with opposite sign because of SOC of the corresponding excited states.

This is exactly what is observed in the MCD **C**-term spectrum of complex **1**, where bands 7 and 8 can therefore be assigned to the two Soret transitions (cf. Table 7), which are split by approximately 1000−1500 cm^{-1}. This is also in agreement with the INDO/S-CI calculation on the entire complex **1**, which predicts two Soret components, but their obtained splitting is too small (∼100 cm^{-1}). From the INDO/S-CI results on **1**, mainly four different types of electronic transitions are identified in the energetical region below the Soret band (cf. Figure S7 in the Supporting Information for porphyrin MO labels):

$\pi \rightarrow \pi^{*(1)}$: $A_{2u}\langle 72\rangle$, $B_{2u}\langle 74\rangle \rightarrow E_g\langle 82/83\rangle$ (LUMO)

$CT^{(1)}$: $A_{1u}\langle 79\rangle$, $A_{2u}\langle 81\rangle \rightarrow \pi^*_{v}\_d_{yz}$, $d_{z^2}/d_{xz}\_\pi^*_{h}$

$\pi \rightarrow \pi^{*(2)}$: lower-lying $E_g(\pi) \rightarrow E_g\langle 82/83\rangle$ (LUMO)

$\pi \rightarrow \pi^{*(3)}$: $A_{1u}\langle 79\rangle$, $A_{2u}\langle 81\rangle \rightarrow B_{1u}\langle 84\rangle$

Here, $\pi \rightarrow \pi^{*(1)}$ and $CT^{(1)}$ (which is a porphyrin(π) → NO-(π^*)_iron(d_π) transition) are located closest to the Soret band followed by $\pi \rightarrow \pi^{*(3)}$, which leads to the assignments of bands 6 and 5, as given in Table 7. An additional admixture of $\pi \rightarrow \pi^{*(2)}$, which is distributed over the whole visible spectral range, is probably also present. The larger intensity of band 6 compared to 5 is due to an additional admixture of Soret character. To higher energy of the Soret transition,

(53) Because of a disorder in the crystal, the experimental structure of **1** in ref 27 has a planar TPP ring. This, however, is certainly not the case in the actual complex and, correspondingly, the INDO/S-CI calculations on this structure lead to a wrong ground state. Therefore, the conformation of the TPP ring from the crystal structure of **2** was applied in the TD-DFT calculation for **1**. This contributes to the incorrect calculation of the Soret shift.

bands 9 and 10 are observed, which have predominant charge-transfer character from $A_{1u}\langle 79\rangle$ and $A_{2u}\langle 81\rangle$ to the unoccupied d_{xy} and d_{z^2} orbitals of iron ($CT^{(2)}$; in the coordinate system shown in Figure 4). In the case of complex **2**, the Soret band shows a shift to lower energy,[54] which is predicted by the INDO/S-CI calculations to lead to enhanced mixing with $CT^{(1)}$ and the appearance of three Soret components in the spectrum. In fact, the MCD spectrum is able to resolve these three individual contributions as bands 6a, 7, and 8, as shown in Figure 9. Bands 6 and 5 that are observed to lower energy of the Soret band are assigned in agreement with **1**. To higher energy of the Soret feature, no contribution of $CT^{(2)}$ is predicted because of the fact that both d_{xy} and d_{z^2} orbitals are significantly shifted to higher energy in **2** compared to **1**. Because iron is located closer to the center of the porphyrin ring in **2**, d_{xy} is shifted to higher energy because of an increased antibonding interaction with the porphyrin orbital $B_{1g}\langle 80\rangle$. On the other hand, d_{z^2} is strongly affected by the axial binding of the N-donor ligand (vide supra) and shifted to higher energy.[18]

Assignment of the Q Region. The medium-intense absorption features observed in the Q region of the spectra of both **1** and **2** actually correspond to the vibronic bands Q_v, whereas the Q bands themselves are of quite low intensity (vide supra). This is reproduced by the INDO/S-CI calculations, which do not predict any absorption features of considerable intensity in the Q region or below.[55] Theoretical analysis of the MCD **C**-term intensity of the Q transitions shows that both components Ψ_1^Q and Ψ_2^Q should lead to a pseudo-**A**-term signal in the MCD spectrum. However, because the transition dipole moments of the Q band are quite small, the product $\vec{D}_u^{Q(1)} \times \vec{D}_v^{Q(2)}$ is small and, hence, the Q transitions should also be weak in MCD. As shown in Figures 8 and 9, this is actually the case for both **1** and **2**. For complex **1**, the splitting of the two components of Q is large ($\sim$1800 cm^{-1}), which leads to a pattern where $Q^{(1)}$ (band 1) is followed by its vibronic band $Q_v^{(1)}$ (band 2; both with positive sign) before the second component $Q^{(2)}$ (band 3; negative sign) appears (see Table 7). In contrast, the Q splitting is smaller for **2** ($\sim$700 cm^{-1}) and, hence, the pseudo-**A** signal of Q (bands 2 and 3) is observed before the pseudo-**A** signal of Q_v (bands 3a and 4).

Limitations of the Model. On the basis of the simple D_{4h} model derived above, one would also predict quite similar overall **C**-term intensities for complexes **1** and **2**. However, this does not seem to be the case experimentally.[18] As was already mentioned above, the symmetry of the porphyrin core is actually clearly lower than D_{4h} in these complexes because of the presence of the phenyl substituents, the out-of-plane (oop) distortions of the porphyrin core, and the bent NO ligand. The deviations are especially severe for the 5C complex **1**, where the iron center shows a large displacement out of the porphyrin plane. In such cases, the porphyrin core itself usually shows a significant amount of oop distortion.[56] Importantly, a large oop distortion of the porphyrin ring will have a profound effect on the MCD intensity because it induces oop character to the Soret transitions. This opens up new channels for the MCD intensity because it allows for SOC in the *x* and *y* directions. This connects the d_{z^2} orbital with d_{xz} and d_{yz}, which gives rise to additional contributions to the **C** term. Importantly, these contributions will be very different for **1** and **2** because of the different nature of their SOMOs (cf. Figure 7).

Discussion

In this paper, we have investigated the coordination of N-donor ligands to five-coordinate (5C) iron(II) nitrosyl complexes [Fe(TPP*)(NO)] and how this influences the spectroscopic properties and electronic structures of these systems. From previous studies, it is known that this interaction is weak,[11,14,37] but quantitative information is not available for biologically relevant imidazole-type ligands. Therefore, we have determined binding constants K_{eq} of 1-methylimidazole (MI) and pyridine (Py) to 5C complexes [Fe(TPP*)(NO)] from UV−vis titrations. Corresponding free binding energies $\Delta G°$ range between −1 and −5 kcal/mol (cf. Table 2). From these data, some fundamental relationships can be established: First, the strength of the interaction strongly depends on the basicity of the applied ligand.[37] Hence, MI is a stronger ligand than Py. Second, the phenyl substituents in TPP*-type ligands influence the binding because of steric and electronic effects. Steric effects are introduced by *o*-methyl substitution of the phenyl rings of TPP and lead to a slight increase of the binding constants. This is due to steric shielding of the binding site. Electronic effects are observed for *o*-fluoro-substituted TPP (T*o*-F_2-PP): the corresponding iron(II) porphyrin NO complex (**1-F**) exhibits an 80 times enhanced ligand affinity for MI compared to TPP, which is attributed to the fact that MI has π-donor abilities. To further investigate possible reasons for the enhanced stability of [Fe(T*o*-F_2PP)(MI)(NO)] (**2-F**), we have determined the crystal structure of this compound. However, the obtained structure and N−O stretching frequency are similar to those of [Fe(TPP)(MI)(NO)] (**2**).[14] Hence, although the free binding energy of MI is twice as large in **2-F** as it is in **2**, the properties of the Fe−N−O subunit are not noticeably affected by this change. We have further investigated the binding of N-donor ligands to complexes [Fe(TPP*)(NO)] by ^{1}H NMR titrations. In this way, the spectra of 5C and 6C iron(II) porphyrin NO adducts are assigned for the first time. These studies provide a direct spectroscopic proof that the addition of larger amounts of N-donor ligands to 5C [Fe(TPP*)(NO)] not only leads to

(54) The observed shift of the Soret band to higher energy in **1** compared to **2** is due to a larger splitting between the occupied A_{1u} and A_{2u} and unoccupied E_g orbitals in **1**. This can be traced back to two effects: (a) the different ring conformations in **1** and **2**, which leads to a stabilization of π bonding and a destabilization of π antibonding orbitals in **1** (evidenced by the energy of the A_{1u} orbital, which is nonbonding to iron) and (b) a large shift to lower energy of A_{2u} due to strong mixing with d_{z^2} in **1** (induced by the out-of-plane displacement of iron).

(55) Because standard quantum-chemical methods such as HF, DFT, or CI calculations operate within the Born−Oppenheimer approximation, vibronic features such as Q_v cannot be calculated with these methods.

(56) (a) Spiro, T. G.; Strekas, T. C. *J. Am. Chem. Soc.* **1974**, *96*, 338−345. (b) Hoard, J. L. *Science* **1971**, *174*, 1295.

the formation of the 6C complex [Fe(TPP*)(L)(NO)] but also facilitates the formation of the diamagnetic complexes [Fe(TPP*)$(L)_2$]. Importantly, this indicates that binding of an N-donor ligand *weakens* the Fe−NO bond, which is in agreement with kinetic studies by Kharitonov et al.[57] Our results also show that the degree of denitrosylation is strongly dependent on the employed TPP* (porphyrin) ligand: whereas TPP itself only leads to the formation of small amounts of the bis(N-donor) complex, compounds with the fluoro-substituted ligand To-F_2PP are very susceptible to NO loss. Therefore, the increase in the N-donor binding constant in **1-F** goes along with a decrease in the stability of the Fe−NO bond. This demonstrates the difficulty of synthesizing stable 6C iron(II) porphyrin NO complexes in solution in the absence of excess NO.

The UV−vis and NMR titration experiments show that, although the binding constants of N-donor ligands to 5C iron(II) porphyrin NO complexes are very small, their coordination has a profound effect on the electronic structure of the Fe^{II}−N−O subunit. Using vibrational spectroscopy coupled to normal-coordinate analysis (NCA), the differences in the electronic structures of 5C complex [Fe(TPP)(NO)] (**1**) and 6C complex [Fe(TPP)(MI)(NO)] (**2**) are further evaluated. Because of the size of the systems studied, force constants were obtained using quantum-chemistry-centered (QCC)-NCA. In the case of **1**, ν(N−O) is observed at 1697 cm^{-1} and ν(Fe−NO) at 532 cm^{-1}, which leads to force constants of 12.53 and 2.98 mdyn/Å for these bonds, respectively. Binding of MI weakens the Fe−NO σ bond, as evidenced by the fact that *both* the N−O and Fe−NO bonds become weaker in **2**. In the case of the N−O bond, this is directly evident from the measured N−O stretching frequency of 1630 cm^{-1}, corresponding to a force constant of 11.55 mdyn/Å. The Fe−NO frequency of 440 cm^{-1} is less diagnostic because of extensive mode mixing with the Fe−N−O bend at 530 cm^{-1}, but the NCA force constant of 2.55 mdyn/Å emphasizes this point. On the basis of these experimental findings as well as spin-density distributions evidenced by MCD spectroscopy,[18] DFT calculations can be used to exactly define the electronic structures of these iron(II) porphyrin NO adducts.

The principal bonding scheme of Fe^{II}NO complexes has been described by Enemark and Feltham.[58] These complexes were classified as {FeNO}^{7}, and it was predicted that they show bent Fe−NO units with radical character on the nitrosyl ligand. This description is also applicable to complexes **1** and **2** and explains their basic features. However, this description also leaves room for a large variation of the electronic structure mediated by metal−ligand covalency. In this way, the electronic structure could vary all the way from an $Fe^{III}NO^-$ extreme (as has been shown for nonheme iron(II) NO adducts[59]) on the one side to an $Fe^{I}NO^+$ extreme on the other side, with the Fe^{II}NO(radical) case being intermediate. These possibilities lead to very different spectroscopic properties and reactivities. Hence, a definition of the electronic structures of heme nitrosyls is very important to elucidate their function in biological signaling and catalysis. In this paper, the bonding scheme of the 6C complex **2** is analyzed in detail. Contributions to the Fe−NO bond arise from (a) a σ-donor interaction between the singly occupied π* orbital of NO (α-π^*_h) and the empty d_{z^2} orbital of iron and (b) a medium-strong π-back-bond between the d_{xz} and d_{yz} orbitals of iron and the empty π* orbitals of NO (α-π^*_h, π^*_v). The occupied orbitals of the π back-bond are mostly metal-based and, therefore, the corresponding electrons can be assigned to the metal, leading to a low-spin iron(II) description. As evidenced from the calculated spin densities, the donation from the singly occupied π* orbital of NO into d_{z^2} of iron(II) is limited. Hence, the electronic structure of complex **2** has to be described as the prototype of an Fe^{II}-NO(radical) system. Recently, the electronic structure of the 6C low-spin Fe^{II}NO complex $[Fe(cyclam-ac)(NO)]^+$ has been studied in detail.[60] In this compound, the applied cyclam−ac ligand system provides a planar N_4 donor set like porphyrin. In the axial position, acetate (ac) is bound trans to NO. Interestingly, the observed N−O stretching frequency of 1615 cm^{-1}, the EPR spectrum showing small *g* shifts and hyperfine splittings of the coordinated NO ligand on *g*(mid), and the calculated spin-density distribution in this complex closely resemble the properties of **2**. Hence, in agreement with our analysis for **2**, this complex has also been described as an Fe^{II}NO(radical) system.

As evidenced by the experimental force constants, the main difference in the electronic structures of complexes **1** and **2** relates to the Fe−NO σ bond, which is distinctively stronger for **1**. Because the π back-bond is comparable for **1** and **2**, the increased σ covalency in the case of **1** leads to an electronic structure with noticeable $Fe^{I}NO^+$ character relative to **2**.[18] This does not mean that complex **1** corresponds to the $Fe^{I}NO^+$ limit where the unpaired electron has been completely transferred to the metal center but that this system is somewhat in between, with the unpaired electron being equally distributed over the Fe−NO unit. This electronic structure description is in agreement with (a) spin-density distributions elucidated from MCD spectroscopy,[18] (b) the larger overall *g* shifts obtained from EPR for **1**, (c) the stronger paramagnetic shifts of the pyrrole hydrogens[48] of the porphyrin core observed for complex **1**, and (d) the weaker Fe−NO bond in **2**, as evidenced by the complex's tendency to lose NO. Hence, the obtained bonding descriptions for **1** and **2** presented here are in agreement with all available experimental data. Compared to earlier DFT studies,[17,20] we have now arrived at a quantitative description of NO bonding to ferrous heme centers.

Because the transition from **1** to **2** corresponds to a change in the Fe−NO σ covalency and because covalency is a property that can change gradually, intermediate stages between complexes **1** and **2** should exist. This is indeed the

(57) Kharitonov, V. G.; Sharma, V. S.; Magde, D.; Koesling, D. *Biochemistry* **1997**, *36*, 6814−6818.
(58) Enemark, J. H.; Feltham, R. D. *Coord. Chem. Rev.* **1974**, *13*, 339.
(59) Brown, C. A.; Pavlosky, M. A.; Westre, T. E.; Zhang, Y.; Hedman, B.; Hodgson, K. O.; Solomon, E. I. *J. Am. Chem. Soc.* **1995**, *117*, 715−732.
(60) Serres, R. G.; Grapperhaus, C. A.; Bothe, E.; Bill, E.; Weyhermüller, T.; Neese, F.; Wieghardt, K. *J. Am. Chem. Soc.* **2004**, *126*, 5138−5153.

case. Studies of Scheidt and co-workers[14] have shown that less donating ligands such as 4-methylpiperidine and 4-(dimethylamino)pyridine lead to ν(N−O) of 1642 and 1653 cm^{-1}, respectively. In these cases, the weaker interaction with the iron center is documented by the longer Fe−N bond lengths of 2.29 and 2.28 Å for these ligands, respectively, compared to 2.18 Å for MI. The second important interaction between Fe^{II} and NO corresponds to a π back-bond. The strength of this interaction can also be varied, as shown by Spiro and co-workers,[61] for 5C complexes where the phenyl rings of the TPP ligand carry either electron-withdrawing or electron-donating groups. Importantly, in this case, an inverse correlation of the N−O and Fe−NO bond strengths is observed.

Detailed analysis of the absorption and MCD data of complexes **1** and **2** shows that their electronic spectra are largely dominated by $\pi \rightarrow \pi^*$ transitions of the porphyrin ligand. Hence, the differences in the electronic structures of these complexes are only very indirectly reflected by the observed electronic transitions. The most obvious change is a shift of the Soret band by ∼1000 cm^{-1} to lower energy in **2** compared to **1**. Importantly, the absorption spectra of **1** and **2** alone neither resolve many transitions nor allow for an identification and analysis of the components of the Soret and Q bands. This is solely based on the MCD **C**-term spectra, which again demonstrates the enormous potential of this method. Theoretical analysis shows that both the Soret and Q bands give rise to a pseudo-**A** term in the MCD spectra of **1** and **2** and, hence, they can easily be identified. Because the Soret band has large transition dipole moments, this feature is also intense in the MCD **C**-term spectrum. In contrast, the Q band is weak both in absorption and in MCD. Correlation of the spectroscopic data to TD-DFT and semiempirical INDO/S-CI calculations shows that a simplification of the TPP ligand in **1** and **2** to porphine (i.e., neglect of the phenyl substituents) leads to wrong predictions of the electronic spectra. On the basis of the INDO/S-CI results, a tentative assignment of all transitions identified in the spectra of **1** and **2** is presented. Experimentally, no charge-transfer transition between Fe^{II} and NO is observed. The INDO/S-CI calculations predict a weak d_{xz}, $d_{yz} \rightarrow$ NO(π^*) transition ($\epsilon \sim 500$ M^{-1} cm^{-1}) in the 12 000 cm^{-1} region (below the Q band) for both **1** and **2**.

The results presented in this study have important implications for the modeling of enzymatic ferrous heme nitrosyl species, which are mostly 6C. Hence, corresponding synthetic model complexes also need to be 6C in solution, which, however, is hard to achieve because of the weak binding constants of N-donor ligands trans to NO. Here we show the factors that influence the strength of this interaction, and we have identified a TPP-based ligand (T*o*-F_2PP) that allows for the preparation of 6C iron(II) porphyrin NO adducts in solution when MI is used as the base. However, it is also demonstrated that the systems with enhanced binding constants facilitate NO loss, which is a drawback. Considering the molecular mechanism of NorBC, a number of different proposals are currently discussed in the literature.[62] Because of the large affinity of ferrous heme for nitric oxide,[63] we believe that mechanisms where NO binds exclusively to the nonheme iron center are less likely. Hence, this leaves the mechanism shown in Scheme 1 as the most probable alternative. Importantly, the enhanced radical character of NO in 6C ferrous heme complexes as identified here is advantageous for the central (radical) N−N coupling step in this mechanism, whereas 5C Fe^{II}NO should be less reactive. This is in agreement with recent findings of Wasser et al., who synthesized a structural model for NorBC based on a 5C heme nitrosyl and which does not show any NO reductase activity.[64] However, it should also be noted that not much experimental information is available for the enzyme regarding the coordination number of the ferrous heme *b* NO adduct. EPR experiments under turnover conditions have identified the nonheme iron(II) NO adduct as a high-spin ($S = {}^3/_2$) species, but the information on the heme center is limited.[65] On the basis of the properties of ferrous and ferric heme *b*, it was speculated that the heme nitrosyl intermediate is only 5C,[66] which would be in disagreement with our findings. However, no proof of this hypothesis is provided. On the basis of our results, we propose that this species is actually 6C. In this context, it should also be noted that hemoglobin and myoglobin form 6C nitrosyl adducts and, therefore, this is definitively a mechanistic possibility for NorBC.

Acknowledgment. This work was supported by the Deutsche Forschungsgemeinschaft (DFG; Grant LE 1393/1) and the Fonds der Chemischen Industrie (FCI). Dr. Frank Neese (Max-Planck Institut für Bioanorganische Chemie, Mülheim an der Ruhr, Germany) is acknowledged for recording the MCD spectra of **1** and **2**.

Supporting Information Available: Derivation of the theoretical expression for the **C**-term intensity; figures of the IR and Raman spectra of **1** and **2**, UV−vis absorption spectra of **1-F** and **2-F**, ^{1}H NMR titration of **1** with Pip, MO diagrams of free porphine^{2-} and NO, and MCD spectra of **2** and **2-F**; tables of the MO charge contributions of $\tilde{\mathbf{2}}$, the calculated ^{57}Fe hyperfine parameters, and coordinates of all optimized structures; and crystallographic data of **2-F** (CIF). This material is available free of charge via the Internet at http://pubs.acs.org.

IC050865J

(61) Vogel, K. M.; Kozlowski, P. M.; Zgierski, M. Z.; Spiro, T. G. *J. Am. Chem. Soc.* **1999**, *121*, 9915−9921.
(62) Zumft, W. G. *J. Inorg. Biochem.* **2005**, *99*, 194−215.
(63) Cooper, C. E. *Biochim. Biophys. Acta* **1999**, *1411*, 290−309.
(64) Wasser, I. M.; Huang, H.; Moënne-Loccoz, P.; Karlin, K. D. *J. Am. Chem. Soc.* **2005**, *127*, 3310−3320.
(65) Hendriks, J.; Warne, A.; Gohlke, U.; Haltia, T.; Ludovici, C.; Lübben, M.; Saraste, M. *Biochemistry* **1998**, *37*, 13102−13109.
(66) Moënne-Loccoz, P.; de Vries, S. *J. Am. Chem. Soc.* **1998**, *120*, 5147−5152.
(67) Fadini, A.; Schnepel, F.-M. *Schwingungsspektroskopie*; Thieme Verlag: Stuttgart, 1985.